Institute for Communications and Navigation

High Accuracy Multi-link Synchronization in LTE Downlink

Chen Zhu

A Thesis submitted for the Degree of
Master of Science in Communication Engineering

Institute for Communications and Navigation

Prof. Dr. Christoph Günther

Supervised by Dr. Armin Dammann
Dr. Patrick Henkel

Munich, October, 2011

Institute for Communications and Navigation

Technische Universität München
Theresienstrasse 90
80333 Munich

Acknowledgement

First of all, I would like to express my gratitude to my supervisor Dr. Armin Dammann in German Aerospace Center (DLR) for his patient supervision in the past six months. I have obtained much help and as well as many inspirations and precious advices from him throughout the whole period of my master thesis. His erudition and creativity in research as well as his precision and patience in work have not only provided me supports in my thesis work, but also established a model for students as me.

In addition, I would like to thank my supervisor at Technical University of Munich, Dr. Patrick Henkel, for his consistent help on the topics concerning navigation. He has provided me many useful suggestions in my thesis. I have also benefitted a lot from his creative and hardworking characteristics.

Behind all these, I must express my sincere and great gratitude to Prof. Dr. Christoph Günther for having opened the door of an extremely interesting field to me and providing me the opportunity to work on the topic in DLR. By attending his lecture Satellite Navigation and Differential Navigation, I am deeply attracted by the fascinating area and the chance to work with a group of really talented people led by him.

I am also grateful to my friend Siwei Zhang, who is my classmate in MSCE as well as colleague in DLR when working on the master thesis. We had a lot of inspiring discussion on the topics and the problems we met in the thesis work. The discussion and encouragements to each other is an important booster for my thesis.

In addition, I have gained great help on the thesis from my colleagues in DLR in the past few months, especially from Wei Wang, from whom I learnt a lot on various topics and gained many inspirations to my thesis work. I really appreciate his support on both research and technical point of view. Furthermore, I would like to thank Kaspar Giger for his help in discussing and organization.

Last but most importantly, I can never express enough gratitude to all my family members in China and in Germany for their persistent supports and love to me.

Abstract

In urban or indoor environments, GNSS may not be able to provide navigation service since insufficient number of satellites can be tracked due to obstructions. In such cases, 3GPP-LTE is an ideal supplement or substitution to GNSS, which provides the possibility of accurate synchronization in downlink so that the time of arrival can be estimated for range based positioning. Because all the cells of the system share the same frequency band to achieve high spectrum efficiency, multi-link synchronization in LTE suffers from the problem of inter-cell interference. The interference can be mitigated by utilizing interference cancelation methods such as SIC (Successive Interference Cancelation). However, if the interference is caused by data symbols, the decoding error may propagates in interference cancelation. Such error propagation problem is especially vital at cell edges, where two links have almost the same power. To deal with the condition, a maximum-likelihood estimator is proposed in this work for joint synchronization and power estimation of multiple links, so that the interference among the joint estimated links can be removed. In addition, an explicit relation between the SINR after data-aided interference cancelation and the decoding symbol error rate is derived, and a joint demodulation scheme is utilized to reduce the symbol error rate in cell edge conditions. The joint processing schemes are integrated into the joint-SIC algorithm for multi-link synchronization. The synchronization results are applied to pseudorange calculation in positioning, which has been shown to outperform the state-of-the-art SIC.

Contents

Nomenclature and Abbreviations

Nomenclature

$\mathbb{R}$	Real numbers
$j = \sqrt{-1}$	Imaginary unit
$\Re(z),\ \Im(z)$	Real and imaginary part of variable z
$c = 299792458$ m/s	Speed of light [m/s]
N_{fft}	Number of point of FFT
$\triangle f$	Subcarrier spacing
T_s	Sampling time
K	Number of links
V	Number of jointly estimated links
τ_k	Delay (Time of Arrival) of the k-th link
$\alpha_k \in \mathbb{R}$	Amplitude of the k-th link
$\mathcal{P}$	Power [W]
$n_k \in \mathbb{C}$	Complex noise of the k-th link
σ^2	Power of noise
I	Power of interference
β	Symbol error rate (SER)
Q	Set of modulation constellation with size $\|Q\|$
$a \in Q$	Symbol in modulation constellation
$x(i), s_0(i), d(i)$	The i-th sample of received signal, pilot, and data symbol in time domain
$X(n), S_0(n), D(n)$	Symbol on the n-th subcarrier of received signal, pilot, and data symbol in frequency domain
h	Channel impulse response in time domain
$H(n)$	Channel impact on the n-th subcarrier in frequency domain
$\vec{r}$	Position vector of the receiver [m]
$\vec{r}^{\,k}$	Position vector of transmitter k [m]
ρ^k	Pseudorange of transmitter k to the receiver [m]
$\vec{e}^{\,k}$	Unit vector pointing from transmitter k to the receiver
H	Geometry matrix

Abbreviations

3GPP	3rd Generation Partnership Project
CIR	Channel Impulse Response
CP	Cyclic Prefix
CRLB	Cramér Rao Lower Bound
CSRS	Cell-Specific Reference Signal
DFT	Discrete Fourier Transform
DLL	Delay Locked Loop
FDD	Frequency Division Duplex
FFT	Fast Fourier Transform
GNSS	Global Navigation Satellite System
LTE	Long Term Evolution
OFDM	Orthogonal Frequency Division Multiplexing
OFDMA	Orthogonal Frequency-Division Multiple Access
IBI	Inter-Block Interference
IC	Interference Cancelation
ID	Identity
IFFT	Inverse Fast Fourier Transform
LOS	Line-Of-Sight
MMSE	Minimum Mean Square Error
ML	Maximum Likelihood
MSE	Mean Square Error
NLOS	Non Line-Of-Sight
SIC	Successive Interference Cancelation
PIC	Parallel Interference Cancelation
PRS	Positioning Reference Signal
PSS	Primary Synchronization Sequence
QPSK	Quadrature Phase-Shift Keying
RB	Resource Block
RMSE	Root Mean Square Error
RS	Reference Signal
SER	Symbol Error Rate
SINR	Signal-to-Interference-plus-Noise Ratio
SNR	Signal-to-Noise Ratio
SS	Synchronization Sequence
SSS	Secondary Synchronization Sequence
TDD	Time Division Duplex
TDoA	Time Difference of Arrival
ToA	Time of Arrival

Chapter 1

Introduction

3GPP Long Term Evolution (LTE) is an innovative wireless communication standard, which is generally approved and started to be implemented by the service provider all over the world due to its advantages in performance. As an OFDM (Orthogonal Frequency-Division Multiplexing) based system, LTE is sensitive to timing offset, since every OFDM symbol is processed and decoded on baseband consecutively, so that an inaccurate synchronization causes interblock interference (IBI) from the earlier OFDM symbol, which significantly degrades the performance of the system [1]. A sufficiently long guard interval between OFDM symbols is effective to remove the impact of timing error in decoding. However, the overhead introduced by the long guard interval remarkably decreases the efficiency of the system. Therefore, accurate synchronization is a fundamental issue for OFDM based systems such as LTE.

In addition, in navigation services, it is possible that GNSS receivers are not able to track sufficient satellites in urban areas or indoor environments due to non-line-sight signal or tiny signal power caused by obstructions. In such cases, the widely spreading wireless communication system such as LTE is an ideal supplement or substitution to GNSS. In order to provide a precise range for positioning services, high accuracy timing estimation in synchronization is urgently demanded, which also coincide with the request of communication. Furthermore, the range based positioning algorithm requests pseudorange measurements from multiple links to determine the position of the receiver. Therefore, besides the serving base station, signals from neighboring base stations have to be detected and precisely synchronized.

One of the state-of-the-art synchronization method for OFDM is proposed in [2] by Schmidl and Cox (S&C approach). The approach constructs a reference block with two identical parts, and calculates the differential correlation between the received signal and the delayed version of the signal so that a correlation peak appears when the reference block is reached. By finding the maximum of the correlation output, the timing of the received signal can be estimated. The estimator is robust to carrier frequency offset since the metric is the autocorrelation of two parts of the received signal. However, it can be observed in simulation results that the output

value near the true delay value forms a plateau instead of a peak [2]. To improve the performance, Minn et al. proposed a revised training signal pattern in [3], which increases the amount of repetition blocks while decreases the sample numbers in each block to keep the total amount of reference samples constant. It has been shown that as the increase of the number of repetition blocks, the differential correlation peak becomes steeper. Shi and Serpedin analyzed the signal pattern proposed by Minn et al. and built a corresponding maximum-likelihood estimator in [4].

Both the S&C approach and its improvement methods request training symbols to construct the repetition structure of the signal, which introduces additional overhead. As a feasible solution, van de Beek et al. proposed a maximum-likelihood estimator utilizing the repetition nature of the cyclic prefix in [5]. Nevertheless, the approach performs well only if the cyclic prefix is long enough, which also inducts overheads. To overcome the disadvantage, Berggren and Popovic proposed an approach in [6] utilizing the property of the secondary synchronization sequence, which is a binary sequence defined in LTE downlink for cell search and synchronization. Because the real sequence has symmetry after transformed into time domain by IFFT, a reverse differential correlator can be built to estimate the timing, which is also robust to frequency offset.

After timing acquisition and removing the frequency offset, fine timing estimation can be obtained by cross-correlating the received signal with the reference sequence containing standardized pilots. Depending on the length, bandwidth and power of the pilots, the accuracy of synchronization can be on subsample level, which is already ideal for communication. However, in the application of positioning, 1 time sample in LTE downlink lasts approximately 32.55[ns] which corresponds to a range of 10m. The range error caused by the quantization error can be several meters, which is not negligible. Therefore, frequency-domain correlation is implemented to search the delay continuously in frequency domain instead of discretely in time domain, so that the quantization error can be overcome.

The state-of-the-art synchronization methods are approved to have outstanding performance in single link case. However, in a practical cellular network, the receivers always receive signal from multiple stations. To increase the spectrum efficiency, LTE aims at frequency reuse-1, which indicates that all the cells exploit the same frequency band. As a result, the inter-cell interference is ubiquitous in multi-link case, and significantly degrades the decoding and synchronization performance of the system, especially at cell edges. Furthermore, in the application of navigation, signals from multiple base stations should be detected and accurately synchronized. With the existence of the inter-cell interference, the links with weak power can drown in the signals from the stronger links, which is an urgent problem in multi-link synchronization.

Many interference coordination and cancelation approaches are proposed for scheduling, which are reviewed in detail in [7, 8]. To realize multi-user detection, successive interference cancelation (SIC) is proposed in [9] to eliminate the inter-cell interference by subtracting the regenerated single link signal successively, starting

from the link with strongest power, which is most reliable in synchronization and decoding. Besides, parallel interference cancelation (PIC) is proposed in [10] as a two-stage multi-user detection scheme, which subtracts the estimated signal of all the other links. Divsalar et al. improved the performance by proposing a partial PIC approach which subtracts the soft values instead of hard values [11]. The a priori information of all the other links requested by PIC is usually obtained by SIC, so the performance of SIC plays a significant role in the interference cancelation.

Mensing et al. exploited the SIC in multi-link synchronization and navigation in [12], and showed that the accuracy of pseudorange measurement increases with interference cancelation. However, the gain of using interference cancelation declines for the receiver at the cell edge, where no link has dominant power so that the temporal strongest link in every stage of SIC is synchronized under non-negligible interference. As a result, the regenerated signal is biased in timing so that it cannot be perfectly removed from the total signal, which affects the synchronization of the other links.

In OFDM based systems such as LTE, a pilot symbol modulated on a subcarrier is interfered from the signal from other links on the same subcarrier at the instant, which can be either a pilot or a data symbol. If the interference is caused by data symbols, data from other links should also be canceled in the multi-link synchronization, so the synchronization performance is relevant with the symbol error rate in decoding. If the symbol error rate is high, the residual decoding error can propagate during the interference cancelation, which vitally degrades the performance of the synchronization of other links. Compared with the near station case, the error propagation problem is more considerable when the receiver is at the cell edge, because the two strongest links have similar power level, which results in high decoding error rate from the very beginning. Mensing et al. mentioned the problem in [13], but no quantitative analysis is induced.

The main contributions of this work are

1. Derivation of a quantitative relation between the decoding symbol error rate of the interference link and the synchronization performance change after subtracting the link.

2. Construction of a maximum likelihood estimator which is able to estimate the timing or power of several links jointly, which overperforms the single link estimator when interference exists.

3. Development of joint successive interference cancelation algorithm utilizing joint synchronization.

4. Development of a joint demapping scheme to reduce symbol error rate when interference exists.

In the following chapters, the fundamentals of OFDM and LTE signal structure are introduced in Chapter 2. Chapter 3 reviews the single link synchronization

algorithms and derives the Cramér-Rao lower bound of timing estimated utilizing pilots contained in multiple OFDM symbols. The pilot-caused inter-cell interference cancelation is discussed in Chapter 4, while a joint successive interference cancelation algorithm is proposed based on the joint timing estimator. Chapter 5 concerns the data-caused interference. We derive the relation between the decoding symbol error rate and the change of synchronization performance after subtracting the decoded link. The joint demapping scheme is also proposed. Chapter 6 discusses the impact of the channel as well as channel estimation. Positioning applying the proposed high accuracy multi-link synchronization method is introduced in Chapter 7. Simulation results are provided in corresponding chapters.

Chapter 2

Fundamentals

In this chapter, the fundamentals of OFDM system as well as its signal model is introduced firstly. Then the basic LTE downlink frame structure is presented followed with the standardized pilots, which can be utilized in synchronization.

2.1 OFDM System and Signal Model

Orthogonal Frequency Division Multiplexing (OFDM) is a scheme which modulates data symbols on multiple carriers in frequency domain. It has properties including high spectrum efficiency, robustness to frequency selective fading, low complexity equalization and other advantages. Due to the advantages of OFDM scheme, many wireless communication systems are based on OFDM, e.g. Long Term Evolution (LTE), IEEE 802.11a/g/n(Wi-Fi), and DVB-T, etc.

On the OFDM receiver side, the signal is processed every OFDM symbol, and the window size of the receiver determines the possible time duration of one OFDM symbol T_{ofdm}. To ensure the orthogonality, the spacing between two neighboring subcarriers is determined by

$$\triangle f = \frac{1}{T_{\text{ofdm}}} \tag{2.1}$$

At the transmitter, inverse fast Fourier transform (IFFT) is executed on the data sequence containing information, which are modulated on the subcarriers, so that the digital signal in frequency domain is transformed into a series of discrete samples in time domain. If the bandwidth of the OFDM system is B, then at most N_{fft}-point IFFT can be implemented in which $N_{\text{fft}} = B/\triangle f$. Consequently, the spacing between two neighboring time-domain sample is

$$T_s = \frac{T_{\text{ofdm}}}{N_{\text{fft}}} = \frac{1}{N_{\text{fft}} \triangle f} \tag{2.2}$$

It can be observed that $T_s = 1/B$ so that the spectrum efficiency of OFDM scheme is twice high as double-sideband modulation. If we denote the data symbol modulated

on the n-th subcarrier by $D(n)$, with normalization by $1/\sqrt{N_{\text{fft}}}$ to keep the power of symbol unitary, the time domain digital signal can be written as

$$d(iT_s) = \frac{1}{\sqrt{N_{\text{fft}}}} \sum_{n=-N_{\text{fft}}/2}^{N_{\text{fft}}/2-1} D(n) \mathrm{e}^{j2\pi n \Delta f i T_s}, \quad i = 0, 1, ..., N_{\text{fft}} - 1 \tag{2.3}$$

After IFFT, a guard interval, which is known as cyclic prefix (CP), is added before every OFDM symbol, and afterwards the digital signal is transmitted over the channel. Cyclic prefix is a repetition of the end part of the OFDM symbol, the length of which should be able to provide a sufficient long guard interval to prevent the inter-symbol interference caused by the channel from the earlier OFDM symbol. Representing the channel impulse response (CIR) $h_0(t)$ by N_h taps with delay as sample duration T_s, the discrete channel impulse response is

$$h_0 = [h(0), h(T_s), ...h((N_h - 1)T_s)]^T \tag{2.4}$$

In such case, the cyclic prefix length of the signal should be at least N_h samples to prevent the inter-symbol interference. Denote the signal with cyclic prefix by

$$d^{\text{CP}} = [d_{-N_h}, ...d_{-1}, d_0, d_1, ...d_{N_{\text{fft}}-1}]^T \tag{2.5}$$

with

$$d_i = \begin{cases} d(iT_s), & \text{if} \quad i \geq 0 \\ d((i + N_{\text{fft}})T_s), & \text{if} \quad i \in \{-N_h, -N_h + 1, ..., -1\} \end{cases} \tag{2.6}$$

Under the assumption of perfect synchronization here, the received signal after transmitting over the channel is

$$x(iT_s) = d^{\text{CP}} \star h_0 + n(iT_s) = \sum_{\mathfrak{h}=0}^{N_h} h_0(\mathfrak{h}T_s) d((i - \mathfrak{h})T_s) + n(iT_s) \tag{2.7}$$

As shown in Equation (2.5)-(2.7), by introducing the cyclic prefix, the impact of the channel on the information part varies from linear convolution to cyclic convolution. A cyclic convolution in time domain corresponds to a multiplication

$$X(n) = H(n)D(n) + N(n), \quad n = -\frac{N_{\text{fft}}}{2}, ..., \frac{N_{\text{fft}}}{2} - 1 \tag{2.8}$$

in frequency domain, where

$$\begin{aligned} X(n) &= \frac{1}{\sqrt{N_{\text{fft}}}} \sum_{i=0}^{N_{\text{fft}}-1} x(iT_s) \mathrm{e}^{-j2\pi n \triangle f i T_s} \\ H(n) &= \sum_{\mathfrak{h}=0}^{N_h} h_0(iT_s) \mathrm{e}^{-j2\pi n \triangle f \mathfrak{h} T_s} \\ D(n) &= \frac{1}{\sqrt{N_{\text{fft}}}} \sum_{i=0}^{N_{\text{fft}}-1} d(iT_s) \mathrm{e}^{-j2\pi n \triangle f i T_s} \\ N(n) &= \frac{1}{\sqrt{N_{\text{fft}}}} \sum_{i=0}^{N_{\text{fft}}-1} n(iT_s) \mathrm{e}^{-j2\pi n \triangle f i T_s} \end{aligned} \tag{2.9}$$

Furthermore, by introducing the cyclic prefix, two identical parts exist in one OFDM symbol, which can be utilized in synchronization. The detailed synchronization approaches will be demonstrated in Section 3.1.

With considering the transmission delay and separating the large scale fading effect factor α, which can be regarded as constant value over time duration of one OFDM symbol, from the channel impulse response, the single link signal model at receiver is

$$x(t) = \alpha s(t-\tau) + n(t) = \alpha(h \star d)(t-\tau) + n(t) \tag{2.10}$$

The corresponding baseband signal after sampling is

$$x(iT_s) = \alpha s(iT_s - \tau) + n(iT_s) = \alpha(h \star d)(iT_s - \tau) + n(iT_s) \tag{2.11}$$

The large scale fading effect factor α is mainly related with the transmission power and pathloss in propagation. The pathloss is relevant with the distance between the transmitter and the receiver, and can be concerned as a constant over a short period of time when both transmitter and receiver are with low-speed, which is the scenario in only ground-station-based communication and navigation. The purpose of dividing the channel impulse response $h_0(t)$ into large scale fading effect factor α and normalized $h(t)$ is to independently discuss the influence of power estimation, which is utilized in the interference cancelation in Chapter 4 and 5, and the influence of channel estimation error, which is concerned in Chapter 6. If $h = [1, 0, .., 0]^T$, i.e. $s(iT_s - \tau) = d(iT_s - \tau)$, the channel is simplified to a free space model, in which the only channel impact is the power attenuation caused by pathloss. If the factor α is further set to 1, the model is equivalent to a simplest AWGN channel.

2.2 LTE Downlink Frame Structure

3GPP Long Term Evolution (LTE) is an innovative wireless communication standard which provides the users the peak data rate of 100 Mbit/s in downlink and

50 Mbit/s in uplink. Compared with the traditional 3G UMTS communication network, many innovative techniques are applied, in which the two main core techniques in physical layer are the OFDMA (Orthogonal Frequency-Division Multiple Access) scheme and the MIMO (Multiple-Input and Multiple-Output) technique. OFDMA is the multiple access scheme which provides the accessibility of various users by allocating distinct resource elements, i.e. subcarrier-time block, to them. By introducing OFDMA and MIMO scheme, the data rate of the system can be significantly increased. At the same time, the design of the signal structure is based on OFDM and considered on three dimensions: time, frequency, and antenna port.

2.2.1 Basic Frame Structure

According to the different methods of duplex, two sorts of frames are standardized in LTE, supporting the TDD (Time Division Duplex) and FDD (Frequency Division Duplex) mode respectively. TDD mode duplexes the uplink and downlink by utilizing distinct time interval, while the uplink and downlink signals are allocated on different frequency bands in FDD mode. Compared with FDD, TDD has the advantage that the channel condition for up- and downlink is barely changed so that the symmetric channel state information can be applied at transmitters to execute precoding in MIMO cases, which results in higher throughput. However, TDD has vital problem of interference for the reason that the signals are using the same frequency band. As a result, the FDD mode is applied and implemented more widely in practice in Europe, so the frame structure introduced in this section is based on FDD, i.e. the frame structure "Type 1" [14].

An LTE frame has duration of $T_f = 10$[ms], consisting of 307200 time samples with sampling time T_s. Each frame is divided into 10 subframes, and each subframe contains two time slots. As a result, the slot length is $T_{\text{slot}} = T_f/20 = 15360T_s = 0.5$[ms]. The frame structure is sketched in Figure 2.1.

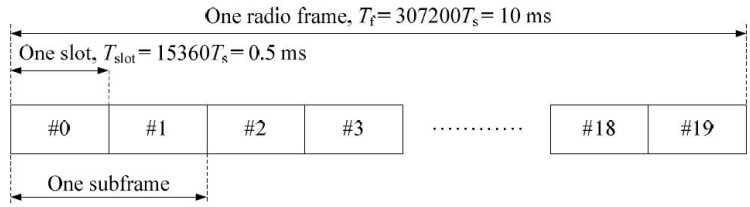

Figure 2.1: LTE frame structure type 1 [14]

As demonstrated in Section 2.1, cyclic prefix(CP) is added before each OFDM symbol as a guard interval so that inter-block interference (IBI) can be avoided if and only if the length of CP is larger than the length of channel impulse response. Consequently, in some particular cases, e.g. channel with long echo path, the length of CP should be larger than ordinary conditions to prevent inter-symbol interference. As a result, two sorts of time slots are provided in LTE downlink, which contains

normal cyclic prefix and extended cyclic prefix respectively. For the slots with extended cyclic prefix, the number of data symbol contained in the slot is reduced due to the increase of CP length. In the following parts, we focus on the slots with normal cyclic prefix, and the detailed signal structure with extended cyclic prefix can be found in [14].

A slot with normal cyclic prefix contains 7 OFDM data symbols with length $N_{\text{fft}}T_s = 2048T_s$ each. Before the first data symbol in every slot, 160 sample-length CP is attached, while 144 sample-length CP is attached in front of other 6 symbols. The subcarrier spacing $\triangle f = 15$[kHz] in such condition so that $T_s = \dfrac{1}{N_{\text{fft}}\ \triangle f} \approx 32.55$[ns]. The subcarriers are grouped into resource blocks as the basic unit of spectrum allocation. Each resource block consists of 12 sequential subcarriers so that the band width of a resource block is $12\ \triangle f = 180$[kHz]. Moreover, although the total allocated bandwidth is $B = N_{\text{fft}} \cdot\ \triangle f \approx 30$[MHz], the maximum feasible bandwidth for data transmission in LTE downlink is 20[MHz], while the marginal parts serve as guard bands. So the maximum number of resource blocks standardized is $N_{\text{max}}^{\text{RB}} = 110$.

The resource elements can be represented in a time-frequency grid as Figure 2.2, in which the horizontal axis denotes the OFDM symbols sequentially in time domain and the vertical axis denotes the subcarriers. On each resource element (l, n), a pilot symbol or data symbol can be allocated. For an OFDM slot utilizing maximum achievable bandwidth, the index range of the available resource elements is $l = 0, 1, ..., 6$, $n = -\frac{N_{\text{fft}}}{2}, ..., \frac{N_{\text{fft}}}{2} - 1$.

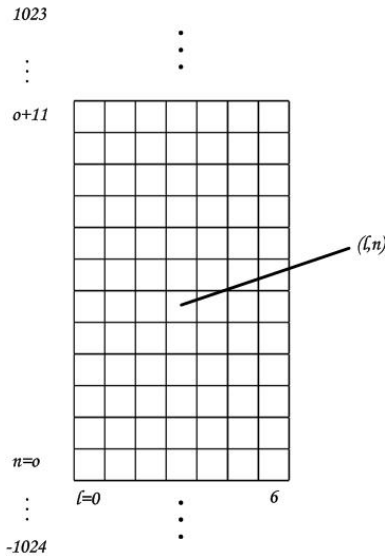

Figure 2.2: Grid represented LTE slot

2.2.2 Synchronization Sequences

In LTE downlink, specific pilots are designed for initial cell search and synchronization, which are known as the synchronization sequences. The synchronization sequences consist of primary synchronization sequence (PSS) and secondary synchronization sequence (SSS). Both sequences have the length of 62, and are allocated on 62 sequential subcarriers in frequency domain, so that the bandwidth of both synchronization sequences are approximately 1MHz. For transmitters with different cell identities, the generated PSS and SSS are distinct, but the resource elements allocated on are independent of the cell identity. In LTE physical layer, there are 504 unique cell identities, which can be denoted as

$$N_{\mathrm{ID}}^{\mathrm{cell}} = 3N_{\mathrm{ID}}^{(1)} + N_{\mathrm{ID}}^{(2)} \tag{2.12}$$

where $N_{\mathrm{ID}}^{(1)}$ denotes cell identity group, which is in the range of 0 to 167, while $N_{\mathrm{ID}}^{(2)}$ is the cell identity within group with only 3 possible values as 0, 1, and 2.

The primary synchronization sequence is a length-62 Zadoff-Chu sequence [15], which has perfect autocorrelation property, i.e. the autocorrelation function is non-zero at time-shift zero and zero otherwise. The PSS can be constructed by

$$S_0^u(m) = \begin{cases} \mathrm{e}^{-j\dfrac{\pi u m(m+1)}{63}} & m = 0, 1, ..., 30 \\ \mathrm{e}^{-j\dfrac{\pi u (m+1)(m+2)}{63}} & m = 31, 32, ..., 61 \end{cases} \tag{2.13}$$

where the root indices u is determined by the cell identity within group $N_{\mathrm{ID}}^{(2)}$ by following mapping

$$u = \begin{cases} 25, & \text{if } N_{\mathrm{ID}}^{(2)} = 0 \\ 29, & \text{if } N_{\mathrm{ID}}^{(2)} = 1 \\ 34, & \text{if } N_{\mathrm{ID}}^{(2)} = 2 \end{cases} \tag{2.14}$$

As a result, at the receiver side, by cross-correlating the received signal with the three different sequences, $N_{\mathrm{ID}}^{(2)}$ can be detected by searching the correlation peak, which also indicates the timing information.

PSS is mapped onto the subcarriers $n = -31, ..., 30$ of the last symbol, i.e. $l = 6$, of slot 0 and 10 in every OFDM frame.

The secondary synchronization sequence is the scrambling result of the interleaved concatenation of two m-sequences with a scrambling sequence provided by the primary synchronization sequence. As a result, the SSS is a binary sequence, which is dependent on both the cell identity group $N_{\mathrm{ID}}^{(1)}$ and the cell identity within group $N_{\mathrm{ID}}^{(2)}$. The detailed definition of the SSS can be found in [14].

After detecting the cell identity within group by PSS, the cell identity group of the signal can be further determined according to the information of SSS. In

addition, the timing estimation can be improved by combining PSS and SSS after the cell search to synchronize the signal.

SSS is mapped onto the subcarriers $n = -31, ..., 30$ of the second last symbol, i.e. $l = 5$, of slot 0 and 10 in every OFDM frame.

The SSS signal has a unique property that in frequency domain the sequence is binary consisting only real values +1 and -1. As a result, utilizing the property of inverse DFT, which transforms the sequence from frequency domain to time domain by

$$s(i) = \frac{1}{\sqrt{N_{\text{fft}}}} \sum_{n=-\frac{N_{\text{fft}}}{2}}^{\frac{N_{\text{fft}}}{2}-1} S(n) \mathrm{e}^{j\frac{2\pi}{N_{\text{fft}}}in} \tag{2.15}$$

If $\{S(n)\}$ are real numbers, then the transform consequence has the symmetry that

$$s(i) = s^*(N_{\text{fft}} - i) \tag{2.16}$$

The symmetry can be exploited to build a reverse differential correlator for synchronization, which is introduced in Section 3.1 in detail.

2.2.3 Reference Signals

Besides the synchronization sequences, additional pilots are also standardized in LTE, which are known as reference signals.

A universally distributed reference signal in LTE downlink is the cell-specific reference signal, which is originally designed for aiding the cell search and channel estimation. The symbols of cell-specific reference signal are QPSK modulated. The real and imaginary parts of the signals are picked from a generated binary pseudo-random sequence $\{c\}$ according to

$$S_0^{l,n_s}(m) = \frac{1}{\sqrt{2}}(1-2c(2m)) + j\frac{1}{\sqrt{2}}(1-2c(2m+1)), \quad m = 0, 1, ..., 2N^{\text{RB}} - 1 \tag{2.17}$$

where N^{RB} is the number of resource blocks allocated to the user, which fulfills $N^{\text{RB}} \leq N^{\text{RB}}_{\text{max}}$. The initialization of the sequence $\{c\}$ is related to the identity of OFDM symbol containing the reference signal sequence and the cell identity of the transmitter, which follows the relation in Equation (2.18) for slots with normal cyclic prefix.

$$c_{\text{init}} = 2^{10} \cdot (7(n_s + 1) + l + 1)(2N^{\text{cell}}_{\text{ID}} + 1) + 2 \cdot N^{\text{cell}}_{\text{ID}} + 1 \tag{2.18}$$

in which n_s denotes the slot number within a frame and l denotes the OFDM symbol number within the slot. The details regarding the generation of the pseudo-random sequence are inducted in [14].

The mapping of cell-specific reference signal is apparently different from that of synchronization sequences, since the sequence are allocated on every other 6 subcarriers instead of sequential subcarriers. In the one antenna case, the cell-specific reference signals are mapped on the first, i.e. $l = 0$, and the fifth OFDM symbol, i.e.

$l = 4$, in every slot. The sequence spreads over the allocated bandwidth with spacing of 6 subcarriers, and is able to achieve at maximum 20[MHz] effective bandwidth, which is much larger than the 1[MHz] bandwidth of synchronization sequences (PSS and SSS). The allocation of the cell-specific reference signal is sketched in Figure 2.3.

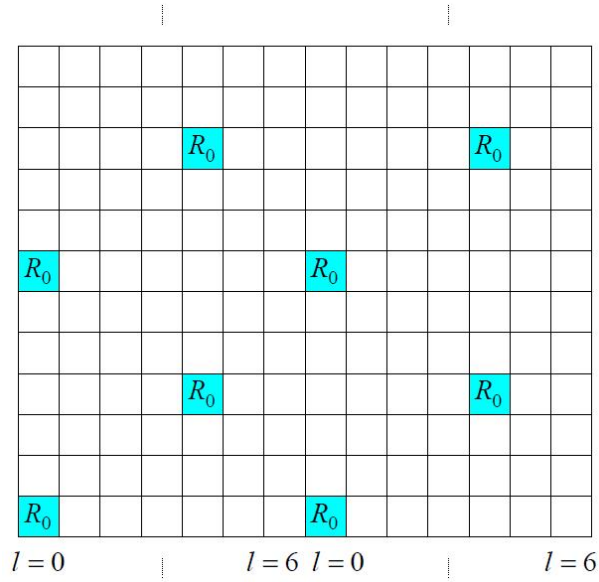

Figure 2.3: Mapping of cell-specific reference signal[14]

The positioning reference signal (PRS) is another pilot defined in LTE downlink, which is designed to provide possibility of high accuracy synchronization for navigation applications. The signal pattern of the positioning reference signal is the same as cell-specific reference signal. The distinction of the two kinds of signals is the different resource element mapping, which also influences the initialization of the pseudorandom sequence as presented in Equation 2.18. In single antenna condition, the positioning reference signals are allocated on OFDM symbols $l = 3, 5, 6$ in the first slot in each subframe, while on OFDM symbols $l = 1, 2, 3, 5, 6$ in the second slot of the subframes. The spacing between two neighboring elements in the sequence is also 6 subcarriers, and the resource elements assigned to synchronization sequences are not allocated with PRS. Figure 2.4 illustrates the mapping of the positioning reference signal.

Positioning reference signal can be distinguished from cell specific reference signal by the property that as a pilot for particular application, it appears only in N_{prs} consecutive subframes out of the whole frame. It is indicated in the standard that the possible values of N_{prs} are 1,2,4, and 6 [16].

It should be also mentioned that the allocation of the reference signals on subcarriers depends on the cell identity of the transmitter, which shifts the mapped

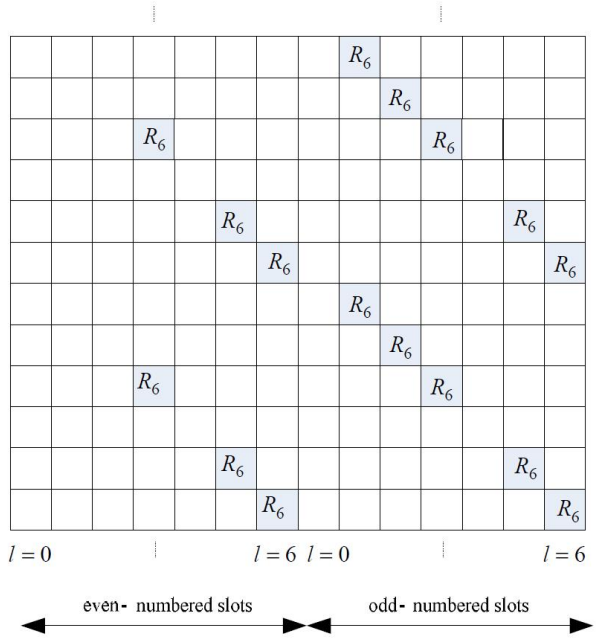

Figure 2.4: Mapping of positioning reference signal[14]

resource elements by ν_{shift} subcarriers, in which $\nu_{\text{shift}} = N_{\text{ID}}^{\text{cell}} \mod 6$ [14]. Consequently, different cells allocate the reference signals on distinct resource elements instead of seizing the same subcarriers for signals from various cells, which is the condition of the synchronization sequences. Such signal pattern determines that the reference signal pilots can suffer from the inter-cell interference caused by the data, but not the pilots of other cells, which would be further discussed in Chapter 5.

Figure 2.5 illustrates the allocation of different kinds of pilots in an instance of LTE downlink frame. In the figure, the grids with blue and green color denotes the synchronization sequences while the yellow and red color denotes the reference signals. It is shown that the synchronization sequences are allocated only on subcarriers with indices between -31 and +30, which corresponds to 1[MHz] bandwidth. Nevertheless, the effective bandwidth of reference signals can be up to 20[MHz], which is much higher than that of synchronization sequences.

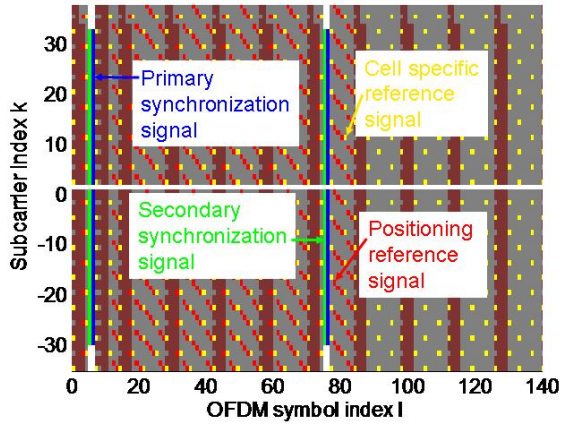

Figure 2.5: Pilots in OFDM downlink signal[17]

Chapter 3

Single-link Synchronization in LTE downlink

In the synchronization of LTE, by utilizing the repetition pattern in the downlink signal, the start of the data frame can be coarsely located in the received signal. Furthermore, the timing can be finely estimated by applying pilot-aided synchronization. The variance of the residual error of the timing estimation is bounded by the Cramér-Rao lower bound (CRLB), which can be regarded as an evaluation of the estimator performance.

In this chapter, the state-of-the-art timing estimation algorithms in OFDM system are reviewed. Additionally, the Cramér-Rao lower bound of the timing estimation exploiting reference sequence containing pilots is derived.

3.1 Synchronization Algorithms in OFDM System

The synchronization in OFDM based systems can be divided into two phases. The first phase is timing acquisition, which makes an approximate estimation of the timing to find the start of the signal. Afterwards, the fine timing estimation and tracking is implemented to achieve high accuracy. Using the baseband signal model demonstrated in Equation (2.11), we can separate the delay τ into integer and fractional parts as in Equation (3.1).

$$\tau = i_0 T_s + \tau_\epsilon \tag{3.1}$$

Consequently, if the fractional part of the delay is ignored, the baseband signal can be simplified to

$$x(i) = \alpha s(i - i_0) + n(i) \tag{3.2}$$

The goal of the timing acquisition is to estimate i_0 or the range of i_0 with bounded error, while a more precise estimate of i_0 is obtained in the fine timing estimation. Demanded by the high accuracy application such as navigation, the fractional part of the delay τ_ϵ should also be estimated.

One of the state-of-the-art timing acquisition algorithm in OFDM is proposed by T.M. Schmidl and D.C. Cox in [2] (S&C approach). The S&C approach is based on differential correlation utilizing the repetitive pattern of the signal. In Schimidl and Cox's method, two identical parts with $N_{\text{fft}}/2$ time samples are constructed at the beginning of the frame as reference block by setting the symbols modulated on every other subcarrier to 0 as in Equation (3.3).

$$S(n) = \begin{cases} D(n), & \text{if } n \text{ is even} \\ 0, & \text{if } n \text{ is odd} \end{cases} \tag{3.3}$$

where $n = -\frac{N_{\text{fft}}}{2}, ..., \frac{N_{\text{fft}}}{2} - 1$. The reference OFDM symbol is transformed to time domain samples by implementing IFFT as

$$\begin{aligned} s(i) &= \frac{1}{\sqrt{N_{\text{fft}}}} \sum_{n=-\frac{N_{\text{fft}}}{2}}^{\frac{N_{\text{fft}}}{2}-1} S(n) \mathrm{e}^{j2\pi \frac{n}{N_{\text{fft}}} i} \\ s(i + \frac{N_{\text{fft}}}{2}) &= \frac{1}{\sqrt{N_{\text{fft}}}} \sum_{n=-\frac{N_{\text{fft}}}{2}}^{\frac{N_{\text{fft}}}{2}-1} S(n) \mathrm{e}^{j(2\pi \frac{n}{N_{\text{fft}}} i + n\pi)} \end{aligned} \tag{3.4}$$

According to Euler's formula,

$$\mathrm{e}^{jn\pi} = \cos(n\pi) + j\sin(n\pi) = \begin{cases} 1, & \text{if } n \text{ is even} \\ -1, & \text{if } n \text{ is odd} \end{cases} \tag{3.5}$$

By combining Equation (3.3) and (3.5), it can be obtained that

$$\begin{aligned} S(n)\mathrm{e}^{jn\pi} &= \begin{cases} D(n), & \text{if } n \text{ is even} \\ 0, & \text{if } n \text{ is odd} \end{cases} \\ &= S(n) \end{aligned} \tag{3.6}$$

As a result, the time domain signal is repetitive, i.e. $s(i) = s(i + \frac{N_{\text{fft}}}{2})$, for $i = i_0, i_0+1, ..., i_0+\frac{N_{\text{fft}}}{2}-1$. There are two identical parts in the received frame satisfying that

$$s(i_0 + \kappa) = s(i_0 + \kappa + \frac{N_{\text{fft}}}{2}), \quad \kappa = 0, ..., \frac{N_{\text{fft}}}{2} - 1 \tag{3.7}$$

Implementing a differential correlator as in Figure 3.1 to process the received signal, a non-coherent estimator can be constructed by

$$\hat{i}_0 = \arg\max_{\tilde{i}_0} \|\Gamma(\tilde{i}_0)\| \tag{3.8}$$

where

$$\Gamma(\tilde{i}_0) = \frac{\sum_{\kappa=\tilde{i}_0}^{\tilde{i}_0+N_{\text{fft}}/2-1} x(\kappa+\frac{N_{\text{fft}}}{2})x^*(\kappa)}{\sum_{\kappa=\tilde{i}_0}^{\tilde{i}_0+N_{\text{fft}}/2-1} \left\|x(\kappa+\frac{N_{\text{fft}}}{2})\right\|^2} \tag{3.9}$$

Consequently, a coarse estimate of the timing can be obtained by searching the peak

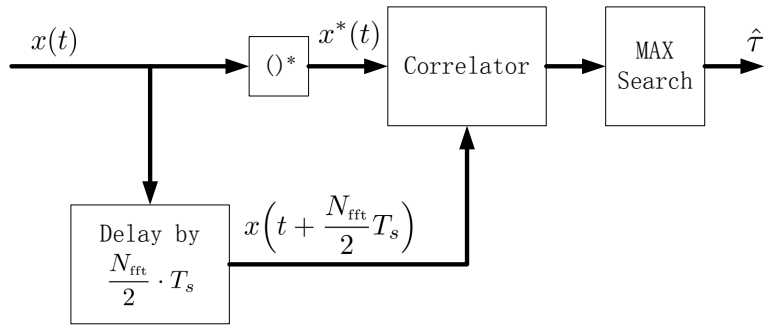

Figure 3.1: Flow chart of an implementation of S&C approach

of the differential correlator. However, it can be observed in the simulation result that the output value is flat around the true delay [2, 1], i.e. a plateau can be found instead of a peak, which degrades the performance. To improve the performance, other reference blocks are designed in [3, 4], which increases the amount of repetition blocks while decreases the sample numbers in each block to keep the total amount of reference samples constant. The metric peak is shown to be sharpened by applying these innovative signal patterns.

The S&C approach is capable to coarsely estimate the timing of the received signal, and the metric it inducts is not affected by the carrier frequency offset, since the both inputs of the correlator are from the received signal and a non-coherent estimation is implemented. Therefore, the S&C approach is effective in timing acquisition. However, the method requests a reference OFDM symbol with half of the subcarriers set to 0, which introduces additional overhead, and makes the power spectrum fluctuated.

As a substitutional solution, the repetition nature of the cyclic prefix can be utilized to implement the differential correlator. Van de Beek et al. proposed a maximum-likelihood estimator utilizing the repetition nature of the cyclic prefix in [5]. Nonetheless, the channel impact makes the first a few samples of cyclic prefix and the corresponding symbol part no longer identical, since the signals before them are distinct. If the channel impulse response lasts N_h samples, and the cyclic prefix length is N_{CP}, the length of identical part in each OFDM symbol is actually $N_{\text{CP}} - N_h$, which is a quite small number in most cases, because increasing the length of cyclic prefix results in additional overhead. Therefore, the method of using the

repetition nature of cyclic prefix does not perform well in timing acquisition of LTE. To overcome the disadvantage of the S&C approach, a reverse differential correlation based approach is proposed in [6] for LTE downlink.

In LTE downlink signal, the secondary synchronization sequence (SSS) is defined for cell search and synchronization, which is a binary sequence. In Section 2.2.2, it is presented that due to the real nature of the SSS signal, the signal in time domain after IFFT has symmetric property that

$$s(i) = s^*(N_{\text{fft}} - i), \quad i = 0, ..., N_{\text{fft}} - 1 \tag{3.10}$$

since

$$\begin{aligned} s(i) =& \frac{1}{\sqrt{N_{\text{fft}}}} \sum_{n=-\frac{N_{\text{fft}}}{2}}^{\frac{N_{\text{fft}}}{2}-1} S(n) \mathrm{e}^{j\frac{2\pi}{N_{\text{fft}}}in} \\ =& \frac{1}{\sqrt{N_{\text{fft}}}} \sum_{n=-\frac{N_{\text{fft}}}{2}}^{\frac{N_{\text{fft}}}{2}-1} S(n) \mathrm{e}^{-j(2\pi n - \frac{2\pi}{N_{\text{fft}}}in)} \\ =& \frac{1}{\sqrt{N_{\text{fft}}}} \sum_{n=-\frac{N_{\text{fft}}}{2}}^{\frac{N_{\text{fft}}}{2}-1} S^*(n) \mathrm{e}^{-j\frac{2\pi}{N_{\text{fft}}}n(N_{\text{fft}}-i)} \\ =& s^*(N_{\text{fft}} - i) \end{aligned} \tag{3.11}$$

The property is utilized by F. Berggren and B.M. Popovic[6] to build a reverse differential correlator that

$$\Gamma_{\text{R}}(\tilde{i}_0) = \frac{\sum_{\kappa=\tilde{i}_0}^{\tilde{i}_0+N_{\text{fft}}/2-1} x(\kappa)x(N_{\text{fft}} - \kappa)}{\sum_{\kappa=\tilde{i}_0}^{\tilde{i}_0+N_{\text{fft}}/2-1} \left\|x(\kappa)\right\|^2} \tag{3.12}$$

Therefore, the timing can be estimated by

$$\hat{i}_0 = \arg\max_{\tilde{i}_0} \left\|\Gamma_{\text{R}}(\tilde{i}_0)\right\| \tag{3.13}$$

The same as S&C approach, the reverse differential correlation estimator is also non-coherent and robust to carrier frequency offset. Moreover, as long as the cyclic prefix length is greater than the length of channel impulse response, the method is not affected by the channel impacts. Further details of the implementation and the application of the approach in cell search can be retrieved in [6, 17].

As a result, exploiting the real nature of the SSS signal, the timing can be estimated utilizing the reverse differential correlator. The approach can achieve similar

performance as the state-of-the-art differential correlation method but without introducing additional reference signal.

After obtaining a coarse estimate of the time of arrival in the acquisition phase, fine timing estimation can be implemented to achieve a more accurate timing. Delay locked loop (DLL) is widely used in timing tracking of GNSS systems and synchronization in some wireless communication applications [18]. DLL is a close-loop controller which adjusts the delay of the signal according to the output of a discriminator to track the timing of the signal. Due to the induction of the close-loop control, DLL can stably and consistently track the timing with high accuracy. However, DLL is sensitive to multipath effect, because the output of the correlation in the discriminator is biased if multipath exists. Moreover, it is difficult to equalize the channel in a sequential tracking loop for continuous signal. In the ground station based system such as LTE, the multipath is ubiquitous and with strong power level, so the bias in synchronization by DLL is vital. Nevertheless, as introduced in Section 2.1, the OFDM based system provides the convenience in channel estimation, so the received signal is usually sampled and processed on baseband, where is feasible to implement channel estimation, to achieve high accuracy timing estimation.

Assuming that the frequency offset f_ϵ has been tracked and eliminated after the acquisition, and the channel estimation is executed to equalize the channel, then the timing can be estimated by cross correlation between the received signal $x(i)$ and the channel-pre-distorted reference signal containing known pilots $s(i) = (h \star s_0)(i)$ spreading over M OFDM symbols. The cross correlator can be constructed as

$$\Gamma_{\mathrm{C}}(\tilde{i}_0) = \frac{\sum_{i=0}^{M\cdot N_{\mathrm{fft}}-1} s(i)x^*(i+\tilde{i}_0)}{\sum_{i=0}^{M\cdot N_{\mathrm{fft}}-1} \left\|s(i)\right\|^2} \tag{3.14}$$

The timing can be estimated by

$$\hat{i}_0 = \arg\max_{\tilde{i}_0} \Re\left(\Gamma_{\mathrm{C}}(\tilde{i}_0)\right) \tag{3.15}$$

The accuracy of the cross-correlation-based method depends on the amount of the pilots exploited as well as the power and spectrum allocation of the pilots. The precision of the timing estimation can be measured by the Cramér-Rao Lower Bound (CRLB), which is elaborately introduced in Section 3.2. When the power and allocation of the pilots are delicately-designed, the CRLB of the timing estimation can be lower than the spacing between two time samples, which is approximately $T_s = \frac{1}{N_{\mathrm{fft}}\Delta f} = \frac{1}{2048*15\mathrm{kHz}} \approx 32.55\times[\mathrm{ns}]$ in ordinary frame of LTE downlink. Under such circumstances, the lower bound cannot be reached due to the quantization error caused by the sampling-time-constraint timing resolution. The integer part of the timing is perfectly estimated in such condition, i.e. $\hat{i}_0 = i_0$, but the fractional part

τ_ϵ is unestimated so that it generates a quantization noise uniformly distributed in the interval $-\frac{T_s}{2}$ to $\frac{T_s}{2}$. The variance of the quantization error is

$$\mathcal{E}[\ n_q n_q^*\ ] = \int_{q=-\frac{T_s}{2}}^{\frac{T_s}{2}} q^2 p(n_q = q) dq = \frac{1}{T_s}\frac{q^3}{3}\Big|_{-\frac{T_s}{2}}^{\frac{T_s}{2}} = \frac{T_s^2}{12} \tag{3.16}$$

Therefore, the root mean square error (RMSE) created by the quantization error is $\frac{1}{\sqrt{12}} T_s \approx 9.4$[ns]. In most communication applications, the accuracy is ideal enough to decode the information bits with the help of cyclic prefix. However, in the navigation applications, the error of 9.4[ns] in time-of-arrival (ToA) measurement results in approximately 2.8[m] error in pseudorange measurement, which is intolerable to precision positioning services. Hence in navigation applications, the sub-sample accuracy should be achieved.

To remove the impact of the sampling time resolution, interpolations can be applied in time domain. More efficiently, the frequency domain cross correlation can be implemented instead of the time domain correlation with sub-sample interpolation. According to the property of the OFDM system, the delay τ_ϵ in time domain is transformed to a phase shift $\mathrm{e}^{-j2\pi n \Delta f \tau_\epsilon}$ of the symbol on the n-th subcarrier in frequency domain, for $n = -\frac{N_{\text{fft}}}{2}, ..., \frac{N_{\text{fft}}}{2}$. As a result, the fractional part of delay can be estimated by searching the optimal of the correlation result between the received signal and the phase-shifted reference sequence, as shown in Equation (3.17).

$$\hat{\tau}_\epsilon = \arg\max_{\tilde{\tau}_\epsilon} \Re\left(\Gamma_{\mathrm{F}}(\tilde{\tau}_\epsilon)\right) \tag{3.17}$$

in which the correlation output

$$\Gamma_{\mathrm{F}}(\tilde{\tau}_\epsilon) = \sum_{u=0}^{M-1} \sum_{n=-\frac{N_{\text{fft}}}{2}}^{\frac{N_{\text{fft}}}{2}-1} S_u(n) \mathrm{e}^{-j2\pi n \Delta f \tilde{\tau}_\epsilon} X_u^*(n) \tag{3.18}$$

where $\{S_u(n)\}$ and $\{X_u(n)\}$ are the u-th OFDM symbol in frequency domain, which are transformed from time domain signal $s(i)$ and $x(i)$ respectively with index range $i = uN_{\text{fft}}, ..., (u+1)N_{\text{fft}} - 1$.

In the frequency-domain correlation, the delay $\tilde{\tau}_\epsilon$ is a continuous variable instead of a discrete variable $\tilde{i}_0$ in time-domain correlation, so the quantization error can be eliminated. To solve the optimization problem, state-of-the-art numeric optimization algorithms such as the golden section search [19] can be implemented.

The performances of time- and frequency-domain correlation are compared in the Figure 3.2. The simulation utilizes the positioning reference signal as the pilot and the perfect channel estimation is assumed. It can be observed that by applying the frequency-domain correlation, the saturation of estimation accuracy inducted by the quantization noise in time-domain cross correlation based method is eliminated.

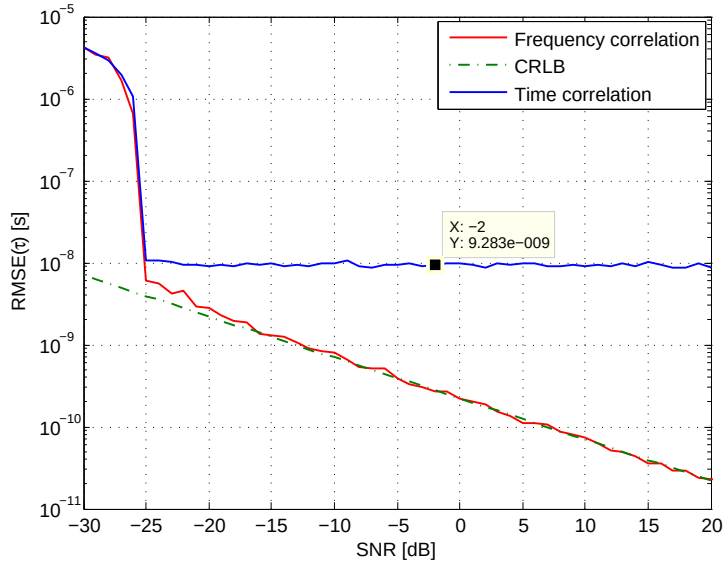

Figure 3.2: Performance comparison between frequency- and time-domain correlation

3.2 Cramér-Rao Lower Bound of Pilot-aided Synchronization

Cramér-Rao lower bound (CRLB) is the lower bound of the variance of the estimated parameter, which can be utilized to evaluate the performance of an estimator. It has been derived in [20] that for a scalar parameter ζ, the CRLB of the estimated $\hat{\zeta}$ according to observation vector y can be expressed as

$$\mathrm{var}[\ \hat{\zeta}(y)\ ] \geq \frac{\left\| \frac{d}{d\zeta} \mathcal{E}[\ \hat{\zeta}(y)\ ] \right\|^2}{\mathcal{E}\left[\ \left\| \frac{d}{d\zeta} \ln\left(p(y|\zeta)\right) \right\|^2 \right]} = \mathrm{CRLB}(\zeta) \tag{3.19}$$

If the estimator is unbiased, $\mathcal{E}[\ \hat{\zeta}(y)\ ] = \zeta$, so the bound can be simplified to

$$\mathrm{var}[\ \hat{\zeta}(y)\ ] \geq \frac{1}{\mathcal{E}\left[\ \left\| \frac{d}{d\zeta} \ln\left(p(y|\zeta)\right) \right\|^2 \right]} = \frac{1}{-\mathcal{E}\left[\ \frac{d^2}{d\zeta^2} \ln(p(y|\zeta))\ \right]} = \mathrm{CRLB}(\zeta) \tag{3.20}$$

For a scaler parameter τ, which is the delay to be estimated in synchronization with the assumption of AWGN channel, it is shown in [20] that the Cramér-Rao lower bound(CRLB) of τ can be expressed as

$$\mathrm{var}[\ \tau\ ] \geq \frac{\sigma^2}{2 \sum_{i=0}^{M \cdot N_{\mathrm{fft}}-1} \left\| \frac{d}{d\tau} s(iT_s - \tau) \right\|^2}, \tag{3.21}$$

where σ^2 is the complex noise power level, and M denotes the number of consecutive OFDM symbols utilized in the estimation, i.e. in total MN_{fft} time samples are used to calculate the log-likelihood function in Equation (3.20). If we denote the subcarrier spacing in frequency domain by $\triangle f$, and the sampling time by $T_s = \frac{1}{N_{\text{fft}} \triangle f}$, according to the property of OFDM, the baseband signal $s(iT_s - \tau)$ can be represented as

$$s(iT_s - \tau) = \frac{1}{\sqrt{N_{\text{fft}}}} \sum_{n=-\frac{N_{\text{fft}}}{2}}^{\frac{N_{\text{fft}}}{2}-1} S_i(n) \mathrm{e}^{j2\pi n \triangle f (iT_s - \tau)} \tag{3.22}$$

For time samples of the same OFDM symbol, the symbols in frequency domain are the same but only with different phase shift depending on the time instance. If we assume M consecutive and complete OFDM symbols are utilized, and the first time sample with index $i = 0$, then the signal in the frequency domain holds the property that

$$S_i(n) = S_u(n), \quad \text{for } i = N_m, N_m + 1, ..., N_m + N_{\text{fft}} - 1 \tag{3.23}$$

where $u = 0, ..., M - 1$ denotes the identity of the OFDM symbol in all M symbols, and $N_m = uN_{\text{fft}}$ denotes the total amount of samples before the u-th OFDM symbol.

It is derived in [20] that if $M = 1$, i.e. in single OFDM symbol case, the CRLB of the delay can be expressed as

$$\text{var}[\ \hat{\tau}\ ] \geq \text{CRLB}(\hat{\tau}) = \frac{\sigma^2}{8\pi^2\ \triangle f^2 \sum_{n=-\frac{N_{\text{fft}}}{2}}^{\frac{N_{\text{fft}}}{2}-1} n^2 \|S(n)\|^2} \tag{3.24}$$

in which $S(n)$ is generally the pilot signal allocated on the n-th subcarrier of the OFDM symbol, which is utilized in the synchronization. It can be noticed that the CRLB of the timing estimation in OFDM system is inversely proportional to the SNR of the signal, and is related with the allocation of the signal power. If the total signal power for transmitting an OFDM symbol is constant, the estimation accuracy is increasingly related with the amount of power allocated on the subcarriers with higher frequency, i.e. greater subcarrier index.

However, for estimation with multiple OFDM symbols, the power utilized for different symbols may change over time. Moreover, the allocation of the pilot signals changes in distinct OFDM symbols, which is the case for reference signals in LTE downlink. Therefore, a CRLB expression for multiple symbols is demanded, which considers the signal changes between different OFDM symbols.

To calculate the CRLB by Equation (3.21), we can calculate the derivative

$$\begin{aligned}\frac{d}{d\tau}s(iT_s-\tau) &= \frac{d}{d\tau}\frac{1}{\sqrt{N_{\text{fft}}}}\sum_{n=-\frac{N_{\text{fft}}}{2}}^{\frac{N_{\text{fft}}}{2}-1} S_i(n)\mathrm{e}^{j2\pi n\triangle f(iT_s-\tau)} \\ &= j\frac{-2\pi\ \triangle f}{\sqrt{N_{\text{fft}}}}\sum_{n=-\frac{N_{\text{fft}}}{2}}^{\frac{N_{\text{fft}}}{2}-1} nS_i(n)\mathrm{e}^{j2\pi n\triangle f(iT_s-\tau)}\end{aligned} \tag{3.25}$$

as well as its norm-2

$$\begin{aligned}\left\|\frac{d}{d\tau}s(iT_s-\tau)\right\|^2 &= \frac{4\pi^2\ \triangle f^2}{N_{\text{fft}}}\sum_n nS_i(n)\mathrm{e}^{j2\pi n\triangle f(iT_s-\tau)}\sum_m mS_i^*(m)\mathrm{e}^{-j2\pi m\triangle f(iT_s-\tau)} \\ &= \frac{4\pi^2\ \triangle f^2}{N_{\text{fft}}}\sum_n\sum_m mnS_i^*(m)S_i(n)\mathrm{e}^{j\frac{2\pi}{N_{\text{fft}}}(n-m)i}\mathrm{e}^{j2\pi\triangle f(m-n)\tau}\end{aligned} \tag{3.26}$$

In order to simplify the layout, we have ignored the summation range of subcarrier index n and m in Equation (3.26). If no additional note is provided, in the following derivation the subcarrier index is always from $-\frac{N_{\text{fft}}}{2}$ to $\frac{N_{\text{fft}}}{2}-1$. For the whole sequence with MN_{fft} time samples,

$$\begin{aligned}&\sum_{i=0}^{M\cdot N_{\text{fft}}-1}\left\|\frac{d}{d\tau}s(iT_s-\tau)\right\|^2 \\ =&\frac{4\pi^2\ \triangle f^2}{N_{\text{fft}}}\sum_n\sum_m mn\sum_{i=0}^{M\cdot N_{\text{fft}}-1} S_i^*(m)S_i(n)\mathrm{e}^{j2\pi\triangle f(m-n)\tau}\mathrm{e}^{j\frac{2\pi}{N_{\text{fft}}}(n-m)i} \\ =&\frac{4\pi^2\ \triangle f^2}{N_{\text{fft}}}\sum_n\sum_m mn\sum_{u=0}^{M-1}\sum_{i=0}^{N_{\text{fft}}-1} S_u^*(m)S_u(n)\mathrm{e}^{j2\pi\triangle f(m-n)\tau}\mathrm{e}^{j\frac{2\pi}{N_{\text{fft}}}(n-m)i} \\ =&\frac{4\pi^2\ \triangle f^2}{N_{\text{fft}}}\sum_n\sum_m mn\sum_{u=0}^{M-1} S_u^*(m)S_u(n)\mathrm{e}^{j2\pi\triangle f(m-n)\tau}\underbrace{\sum_{i=0}^{N_{\text{fft}}-1}\mathrm{e}^{j\frac{2\pi}{N_{\text{fft}}}(n-m)i}}_{=N_{\text{fft}}\delta_{mn}}\end{aligned} \tag{3.27}$$

where δ_{mn} is the Kronecker delta function defined as

$$\delta_{mn}=\begin{cases}1 & \text{if}\quad m=n,\\ 0 & \text{otherwise.}\end{cases} \tag{3.28}$$

Consequently, the summation in Equation (3.27) is non-zero only if the subcarrier index fulfills $m=n$ so that the formula can be simplified to

$$\sum_{i=0}^{M\cdot N_{\text{fft}}-1}\left\|\frac{d}{d\tau}s(iT_s-\tau)\right\|^2 = 4\pi^2\ \triangle f^2\sum_{u=0}^{M-1}\sum_n n^2\|S_u(n)\|^2 \tag{3.29}$$

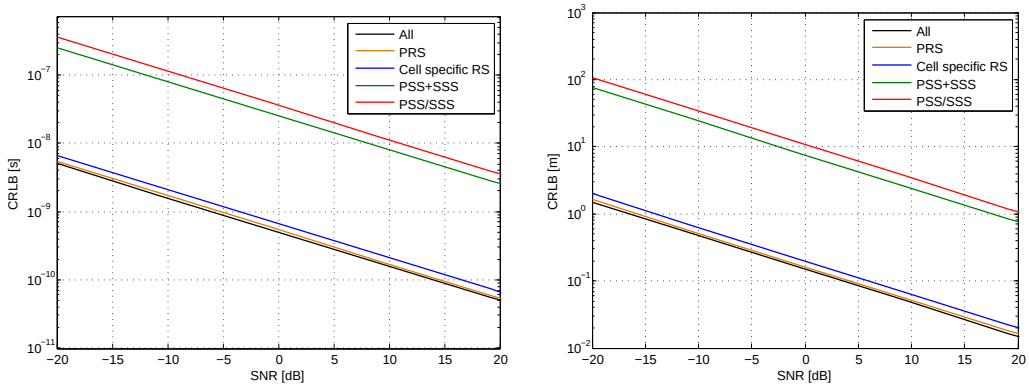

(a) CRLB of time of arrival estimation

(b) CRLB of pseudorange estimation

Figure 3.3: Cramér-Rao lower bounds of synchronization using different pilots

As a result, substituting Equation (3.29) into Equation (3.21), the Cramér-Rao Lower Bound of the timing estimation in AWGN channel by utilizing M OFDM symbols can be obtained by

$$\mathrm{var}[\ \hat{\tau}\ ] \geq \mathrm{CRLB}(\hat{\tau}) = \frac{\sigma^2}{8\pi^2\ \triangle f^2 \sum_{u=0}^{M-1} \sum_{n=-\frac{N_{\mathrm{fft}}}{2}}^{\frac{N_{\mathrm{fft}}}{2}-1} n^2 \|S_u(n)\|^2} \tag{3.30}$$

The Cramér-Rao lower bounds of timing estimation using different pilots standardized in LTE downlink signal are compared in Figure 3.3. In the calculation, a subframe containing 14 OFDM symbols is utilized, and 4 sorts of pilots including primary synchronization sequence (PSS), secondary synchronization sequence (SSS), cell-specific reference signal and positioning reference signal (PRS) are mapped to the corresponding resource elements. The bandwidths of cell-specific reference signal and the positioning reference signal are chosen as the maximum available value 20[MHz]. In the figure, the lowest bound is calculated by utilizing all the four pilots simultaneously. It can be observed that from the CRLB perspective of view, the positioning reference signal achieves best performance in synchronization, while the reference signals significantly outperforms the synchronization sequences due to the much larger bandwidth.

Chapter 4

Pilot-caused Inter-cell Interference Cancelation in Multi-link Synchronization

In the cellular network of LTE, a mobile station can receive downlink signals from more than one base station. If frequency reuse-1 is operated to achieve a high frequency spectrum efficiency, i.e. all the base stations are transmitting downlink signals in the same frequency band, the inter-cell interference from neighboring cells and base stations is unavoidable for all the links, which degrades the performance of timing estimation. Moreover, in order to provide positioning services, the receiver should synchronize the signals from multiple links simultaneously, so the service requests sufficient signal strength from at least three links, which also results in considerable inter-cell interference among different links.

The impact of the interference can be observed from the simplest two station case as in Figure 4.1. According to the curves, the timing estimation accuracy saturates in high SNR region due to the inter-cell interference. If we add the interference power to the noise power level, which provides us the signal-to-noise-plus-interference-ratio (SINR) instead of SNR, then the calculation of Cramér-Rao lower bound exploiting SINR results in a new lower bound with greater value, which reflects the degradation of performance in timing estimation. It can be verified from the curves that when interference is dominant compared with noise, the RMSE of timing estimation with interference exactly touches the bound calculated by SINR.

Therefore, the cancelation or mitigation of the inter-cell interference is essential for high precision multi-link synchronization and the high accuracy positioning in the LTE network.

For the synchronization sequences (PSS and SSS) defined in LTE downlink signals, the occupied resource elements are the same for all the cells and base stations, so that the interference impacting PSS and SSS are also synchronization sequences of other cells. As a certain kind of pilots used for cell search and synchronization of the received signal, the synchronization sequences are known if the corresponding cell

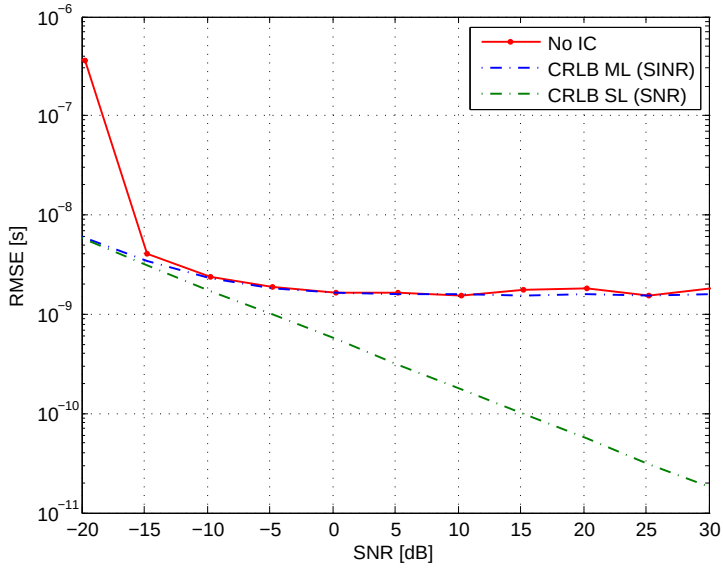

Figure 4.1: Impact of inter-cell interference in two-link synchronization

identity is given. Therefore, as long as the cell identity is detected, the sequence of a certain cell can be subtracted from the superposition signal so that the interference declines for the other cells in the following timing estimation.

In this chapter, the utilization of the state-of-the-art successive interference cancelation (SIC) approach is introduced, and a joint synchronization scheme is proposed. The scheme can be implemented into a joint SIC method in synchronization, which outperforms the SIC approach in accuracy.

4.1 Multi-link Synchronization using Successive Interference Cancelation (SIC)

Denoting the number of base stations by N_{BS} and the number of cells per base station as N_C, the number of links is $K = N_{BS}N_C$. So we have the received signal model as following:

$$x(t) = \sum_{k=1}^{K} \alpha_k s_k(t-\tau_k) + n(t) = \sum_{k=1}^{K} \alpha_k (h_k \star d_k)(t-\tau_k) + n(t) \tag{4.1}$$

where d_k is the transmitted signal from the k-th link while h_k is the corresponding channel impulse response with normalized amplitude, and $\mathcal{P}_k = \alpha_k^2$ is the received power of the k-th link which is related with the large-scale fading, e.g. pathloss, of the channel. The amplitude parameter α_k can be regarded as a constant real value for a short period of time as explained after Equation (2.11). If the timing estimation is implemented by passing the received signal through a correlation bank

with the K corresponding reference signals, the SINR of the k-th link during the correlation process is

$$\mathrm{SINR}_k = \frac{\alpha_k^2}{\sum\limits_{\substack{j\in\{1...K\}\\ j\neq k}} \alpha_j^2 + N_k} \tag{4.2}$$

in which $N_k = \mathcal{E}[\|n(t)\|^2]$ is the noise power of the link. Due to the fact that the summation of reception power from all the links is constant at a time instant, the link with higher reception power is equivalent to higher SINR according to

$$\mathrm{SINR}_k = \frac{\alpha_k^2}{\mathcal{P}_t^2 - \alpha_k^2 + N_k}, \quad \text{where } \mathcal{P}_t^2 = \sum_{k=1}^{K} \alpha_k^2 = \text{const.} \tag{4.3}$$

For the reason that the performance of the estimator is increasingly related with the SINR, a straightforward solution to the interference problem in the multi-link case is the successive interference cancelation (SIC) approach [9], which sorts the links decreasingly according to the estimated power at correlation peaks, and subtracts the reconstructed signal of the current strongest link. As a result, the SIC approach always estimate the most reliable component which has the highest SINR, and the reconstruction as well as the subtraction processing also starts from the most reliable link.

Denote $\{i_1, i_2, ..., i_K\}$ as the indices of the links after sorting, so that

$$\alpha_{i_1}^2 \geq \alpha_{i_2}^2 \geq ... \geq \alpha_{i_K}^2 \tag{4.4}$$

Starting from the link i_1, an estimate of the channel, transmission delay as well as the decoded data can be obtained by applying the reference signal from the corresponding link. Consequently, the signal of the i_1-th link can be regenerated from the estimates and subtracted from the received signal, so that the interference from the current strongest link is canceled or mitigated in the following processing steps.

Initializing the SIC process with the original received signal $x^{(1)}(t) = x(t)$, and assuming that a group of a priori estimate of amplitude is obtained, then at the k-th estimation and reconstruction step,

$$\hat{\tau}_{i_k} = \arg\max_{\tau_{i_k}} \{s_{i_k}(t - \tau_{i_k}) \star x^{(k)}(t)\} \tag{4.5}$$

$$\hat{\alpha}_{i_k} = \frac{\Re\left(\int_0^T s_{i_k}(t - \hat{\tau}_{i_k}) x^{(k)^*}(t) dt\right)}{\int_0^T \|s_{i_k}(t - \hat{\tau}_{i_k})\|^2 dt} \tag{4.6}$$

$$x^{(k+1)}(t) = x^{(k)}(t) - \hat{\alpha}_{i_k} s_{i_k}(t - \hat{\tau}_{i_k}) \tag{4.7}$$

where T is the time duration of the reference signal $s_{i_k}(t)$.

For simplicity, we assume the link indices k are sorted decreasingly with the amplitude of the links, i.e. $\alpha_1 \geq \alpha_2 \geq \cdots \alpha_K$. This assumptions hold throughout the following sections if not stated differently. As a result, Equation (4.5) - (4.7) can be simplified to

$$\hat{\tau}_k = \arg\max_{\tau_k} \{ s_k(t - \tau_k) \star x^{(k)}(t) \} \tag{4.8}$$

$$\hat{\alpha}_k = \frac{\Re\left(\int_0^T s_k(t - \hat{\tau}_k) x^{(k)^*}(t) dt \right)}{\int_0^T \| s_k(t - \hat{\tau}_k) \|^2 dt} \tag{4.9}$$

$$x^{(k+1)}(t) = x^{(k)}(t) - \hat{\alpha}_k s_k(t - \hat{\tau}_k) \tag{4.10}$$

Figure 4.2 illustrates the general process of the SIC approach.

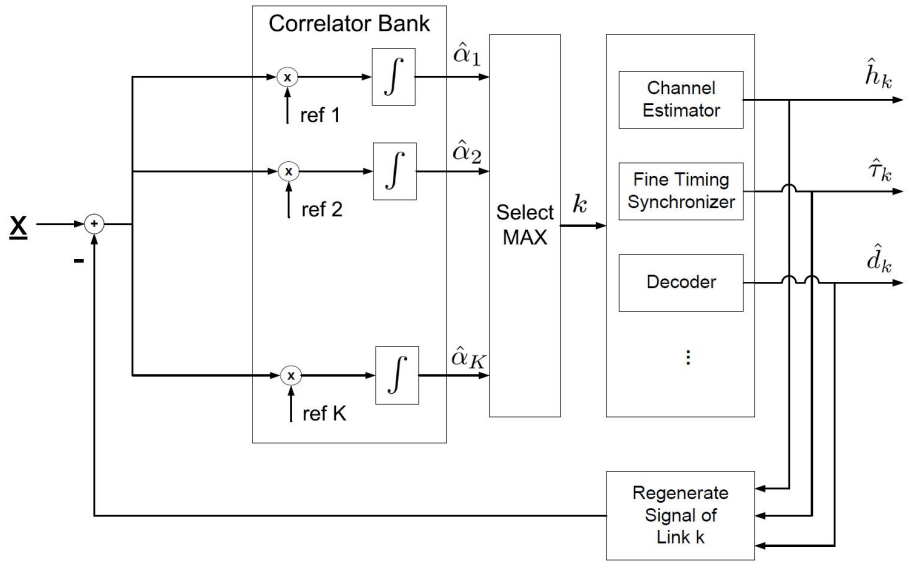

Figure 4.2: Successive interference cancelation approach

In the baseband processing, one can simply replace the continuous signals with the sampled discrete signals, and replace the integral with summation.

Mensing et al. applied the SIC scheme in the multi-link synchronization to mitigate the inter-cell interference to achieve higher accuracy [12]. When the mobile station is close to the serving base station, the serving base station makes the signals from other links drowning in its signal. Nevertheless, the signal from the serving cell can be regenerated reliably due to the strong SINR, so the interference level significantly declines after the cancelation of the strongest-link signal. The comparison of the simulation result with and without SIC in a two-base-station case illustrated in

Figure 4.3. In the simulation, two base stations are set 750[m] away from each other as shown in Figure 4.4, and the mobile station is 350[m] away from the first station. The horizontal axis in Figure 4.3 denotes various signal-to-noise-ratio (SNR) of the received signal from second station by changing noise level, and the vertical axis is the RMSE (Root Mean Square Error) of the timing estimation for the link. It can be seen that SIC can significantly increase the synchronization accuracy for the link with weaker received signal power.

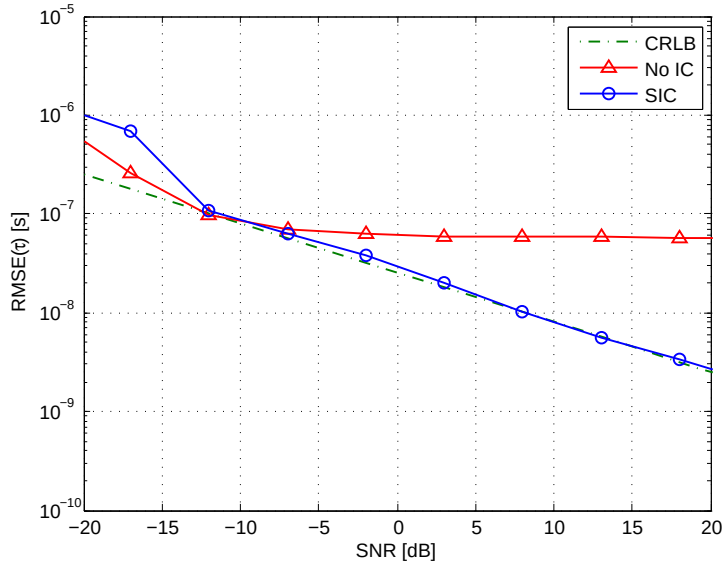

Figure 4.3: Performance of successive interference cancelation

Figure 4.4: Two-base-station simulation scenario

Furthermore, the improvement is much more significant when the mobile station is close to one of the base station than when at the cell edge. One of the reason is that the interference to the weaker link is much more vital for the users near the serving station, so the estimation accuracy improvement is obvious after the synchronization sequence from the stronger station is canceled. The other reason is that the SINR is relatively low for the first estimated link at the cell edge so that the timing estimation is less accurate. Due to the inaccurate timing estimation for the stronger link, the subtracted regeneration of the signal has some time estimation

error, which may degrade the performance. The performance degradation at the cell edge is much more vital when data-caused inter-cell interference exists, because the error rate of the data decoding is quite high even for the strongest link, so that the error propagates in the interference cancelation process. The details would be discussed in Chapter 5.

4.2 Multi-link Synchronization using Joint SIC

4.2.1 Maximum Likelihood Estimation of Parameters from Multiple Links

For mobile stations at the cell edges, it is common that the power of the strongest two links are on the same level. Compared with the near-site condition, in which case only one of the links has dominant power level, the performance of synchronization and other estimation of the strongest link at the cell edge degrades since there is another interferer with similar power. Consequently, if the interference cancelation scheme, e.g. SIC, is utilized, the error propagation results in an even worse performance than directly estimating links without interference cancelation.

To deal with the cell edge interference problem, one possible solution is synchronizing the strong links jointly instead of estimating every link independently. For the reason that the interference is caused by the reference sequences of other cells, all the interference signals affecting the timing estimation, i.e. d_k , are known. If we further assume that channel estimation is perfect, i.e. $\hat{h}_k = h_k$, the parameters to be estimated are the amplitude and time delay of strongest V links, where V is the number of jointly processed links. Therefore, the likelihood function of the received baseband signal after sampling can be written as

$$x(iT_s) = \sum_{k=1}^{K} \alpha_k s_k(iT_s - \tau_k) + n(iT_s) = \sum_{k=1}^{K} \alpha_k (h_k \star d_k)(iT_s - \tau_k) + n(iT_s) \quad (4.11)$$

$$p_X\big(x(iT_s)|\alpha_{1\ldots V}, \tau_{1\ldots V}\big) = \frac{1}{\pi\sigma_{IN}^2}\exp\left(-\frac{1}{\sigma_{IN}^2}\|x(iT_s) - \sum_{v=1}^{V}\alpha_v s_v(iT_s - \tau_v)\|^2\right) \quad (4.12)$$

in which σ_{IN}^2 denotes the power of interference plus noise. We assume that the superposition of the remaining links' signals after channel distortion approximates a Gaussian distribution. Furthermore, obviously, the interference level in joint estimation is lower than that in independent estimation due to

$$\sigma_{IN}^2 = \sum_{k=V+1}^{K} \alpha_k^2 + N < \sum_{k=2}^{K} \alpha_k^2 + N \quad (4.13)$$

For one OFDM symbol including N_{fft} time-domain samples, the noises between

two samples are independent so that

$$p_{\underline{X}}\big(x(iT_s)_{i=0\ldots N_{\text{fft}}-1}|\alpha_{1\ldots V},\tau_{1\ldots V}\big)=\prod_{i=0}^{N_{\text{fft}}-1}p_X\big(x(iT_s)|\alpha_{1\ldots V},\tau_{1\ldots V}\big) \tag{4.14}$$

and the corresponding log-likelihood function is

$$\begin{aligned}&\ln\big[p_{\underline{X}}\big(x(iT_s)_{i=0\ldots N_{\text{fft}}-1}|\alpha_{1\ldots V},\tau_{1\ldots V}\big)\big]\\=&\sum_{i=0}^{N_{\text{fft}}-1}\ln\big[p_X\big(x(iT_s)|\alpha_{1\ldots V},\tau_{1\ldots V}\big)\big]\\=&-N_{\text{fft}}\ln[\pi\sigma_{IN}^2]-\frac{1}{\sigma_{IN}^2}\sum_{i=0}^{N_{\text{fft}}-1}\|x(iT_s)-\sum_{v=1}^{V}\alpha_v s_v(iT_s-\tau_v)\|^2\end{aligned} \tag{4.15}$$

If we use a maximum-likelihood estimator to maximize Equation (4.15), the parameters are estimated according to

$$\begin{aligned}\hat{\alpha}_{1\ldots V},\hat{\tau}_{1\ldots V}&=\arg\min f_0(\alpha_{1\ldots V},\tau_{1\ldots V})\\&=\arg\min\sum_{i=0}^{N_{\text{fft}}-1}\|x(iT_s)-\sum_{v=1}^{V}\alpha_v s_v(iT_s-\tau_v)\|^2\end{aligned} \tag{4.16}$$

It is straightforward that the cost function $f_0(\alpha_{1\ldots V},\tau_{1\ldots V})$ is the superposition of N_{fft} quadratic function of arguments $\{\alpha_v s_v(iT_s-\tau_v)\}$. Globally, the cost function is not convex for the parameters $\alpha_{1\ldots V}$ and $\tau_{1\ldots V}$ as arguments in general. However, if we have a group of a priori estimation of the amplitude α_k, and the search space of the delay is inside ±1 time samples of the true value, it can be verified that the cost function is locally convex. Therefore, we can find the minimum value of the cost function in the time domain, in which case the baseband signal is discrete and the estimation accuracy is bounded by the quantization error as shown in Section 3.1, and then implement multi-dimensional search in frequency domain, where the signal is continuous while the cost function is convex so that state-of-the-art convex optimization algorithms can be utilized.

Actually, when sorting the links according to their power, a coarse estimate of the amplitude of the k-th link $\hat{\alpha}_k$ can be obtained by pre-processing, e.g. independent estimation according to Equation (4.8) and (4.9). As a result, the timing can be estimated assuming that the amplitude of links are known. In this case, the problem can be modified as

$$\hat{\tau}_{1\ldots V}=\arg\min f_0(\tau_{1\ldots V})=\arg\min\sum_{i=0}^{N_{\text{fft}}-1}\|x(iT_s)-\sum_{v=1}^{V}\hat{\alpha}_v s_v(iT_s-\tau_v)\|^2 \tag{4.17}$$

with

$$
\begin{aligned}
& f_0(\tau_{1\ldots V}) \\
&= \sum_{i=0}^{N_{\text{fft}}-1} \|x(iT_s) - \sum_{v=1}^{V} \hat{\alpha}_v s_v(iT_s - \tau_v)\|^2 \\
&= \sum_{i=0}^{N_{\text{fft}}-1} \Big(\|x(iT_s)\|^2 + \sum_{v=1}^{V} \hat{\alpha}_v^2 \|s_v(iT_s - \tau_v)\|^2 - 2\Re\big(\sum_{v=1}^{V} \hat{\alpha}_v s_v(iT_s - \tau_v) x^*(iT_s) \big) \\
&\qquad + \sum_{v=1}^{V} \sum_{\substack{w=1 \\ w \neq v}}^{V} \hat{\alpha}_v \hat{\alpha}_w s_v(iT_s - \tau_v) s_w^*(iT_s - \tau_w) \Big)
\end{aligned}
\tag{4.18}
$$

According to Parseval's law, it can be derived in Equation (4.19) that the power summation over all the time-domain samples of one OFDM symbol equals to the total power of data modulated on all the subcarriers, but independent on the delay.

$$
\sum_{i=0}^{N_{\text{fft}}-1} \|s_v(iT_s - \tau_v)\|^2 = \sum_{n=-N_{\text{fft}}/2}^{N_{\text{fft}}/2-1} \|S_v(n) \mathrm{e}^{-j2\pi n \Delta f \tau_v}\|^2 = \sum_{n=-N_{\text{fft}}/2}^{N_{\text{fft}}/2-1} \|S_v(n)\|^2 \tag{4.19}
$$

Consequently, due to the fact that the transmission power and the received signal power $\|x(iT_s)\|^2$ are independent on the delay of the links, the problem can be simplified to

$$
\hat{\tau}_{1\ldots V} = \arg\min f_\tau(\tau_{1\ldots V}) \tag{4.20}
$$

with

$$
\begin{aligned}
f_\tau(\tau_{1\ldots V}) = \sum_{i=0}^{N_{\text{fft}}-1} \Big(& -2 \sum_{v=1}^{V} \hat{\alpha}_v \Re\big(s_v(iT_s - \tau_v) x^*(iT_s) \big) \\
& + \sum_{v=1}^{V} \sum_{\substack{w=1 \\ w \neq v}}^{V} \hat{\alpha}_v \hat{\alpha}_w s_v(iT_s - \tau_v) s_w^*(iT_s - \tau_w) \Big)
\end{aligned}
\tag{4.21}
$$

According to Equation (4.21), the cost function to be minimized f_τ consists of two parts. The first term is just the summation of the cross-correlation results between the received signal and the reference signal of link v with delay τ_v, and the second term is the corresponding cross terms of every two different links.

As demonstrated in the convexity problem of cost function in Equation (4.16), we can obtain the timing estimates of strongest V links jointly, by finding the minimum value in time-domain with discrete search space and solving the V-dimensional optimization in frequency domain with locally convex cost function.

After obtaining a group of timing estimates $\hat{\tau}_{1\ldots V}$, the amplitude of the links can be further refined. Rewriting the cost function f_0 in Equation (4.16) with delay as

known and amplitude as arguments, we can estimate the amplitudes by minimizing the cost function

$$\begin{aligned}
&f_\alpha(\alpha_{1\dots V}) \\
&= \sum_{i=0}^{N_{\text{fft}}-1} \|x(iT_s) - \sum_{v=1}^{V} \alpha_v s_v(iT_s - \hat{\tau}_v)\|^2 \\
&= \sum_{i=0}^{N_{\text{fft}}-1} \Big(\|x(iT_s)\|^2 + \sum_{v=1}^{V} \alpha_v^2 \|s_v(iT_s - \hat{\tau}_v)\|^2 - 2\Re\big(\sum_{v=1}^{V} \alpha_v s_v(iT_s - \hat{\tau}_v) x^*(iT_s) \big) \\
&\qquad + \sum_{v=1}^{V} \sum_{\substack{w=1 \\ w\neq v}}^{V} \alpha_v \alpha_w s_v(iT_s - \hat{\tau}_v) s_w^*(iT_s - \hat{\tau}_w) \Big)
\end{aligned} \tag{4.22}$$

One necessary condition of finding the minimum of f_α is that the partial derivatives of f_α with respect to arguments $\{\alpha_{1\dots V}\}$ are all zero, i.e. for any v,

$$\begin{aligned}
&\frac{\partial}{\partial \alpha_v} f_\alpha(\alpha_{1\dots V}) \\
&= \sum_{i=0}^{N_{\text{fft}}-1} \Big(2\alpha_v \|s_v(iT_s - \hat{\tau}_v)\|^2 - 2\Re\big(s_v(iT_s - \hat{\tau}_v) x^*(iT_s) \big) \\
&\quad + \sum_{\substack{w=1 \\ w\neq v}}^{V} \alpha_w 2\Re\big(s_v(iT_s - \hat{\tau}_v) s_w^*(iT_s - \hat{\tau}_w) \big) \Big) \\
&\stackrel{!}{=} 0
\end{aligned} \tag{4.23}$$

By writing (4.23) for all $v = 1\dots V$ in matrix form, we obtain a linear function

$$\underbrace{\begin{bmatrix} p_{1,1} & p_{1,2} & \cdots & p_{1,V} \\ p_{2,1} & p_{2,2} & & p_{2,V} \\ \vdots & & \ddots & \vdots \\ p_{V,1} & p_{V,2} & \cdots & p_{V,V} \end{bmatrix}}_{P} \underbrace{\begin{bmatrix} \alpha_1 \\ \alpha_2 \\ \vdots \\ \alpha_V \end{bmatrix}}_{\alpha} - \underbrace{\begin{bmatrix} b_1 \\ b_2 \\ \vdots \\ b_V \end{bmatrix}}_{b} = \begin{bmatrix} 0 \\ 0 \\ \vdots \\ 0 \end{bmatrix} \tag{4.24}$$

It is obvious that $P \in \mathbb{R}^{V\times V}, \alpha \in \mathbb{R}^{V\times 1}, b \in \mathbb{R}^{V\times 1}$, while the elements in the matrix and vectors are

$$\begin{aligned}
p_{v,w} &= \sum_{i=0}^{N_{\text{fft}}-1} \Re\big(s_v(iT_s - \hat{\tau}_v) s_w^*(iT_s - \hat{\tau}_w) \big) \\
b_v &= \sum_{i=0}^{N_{\text{fft}}-1} \Re\big(s_v(iT_s - \hat{\tau}_v) x^*(iT_s) \big)
\end{aligned} \tag{4.25}$$

Because the pilot sequences are well designed, the real part of the cross correlation between two different sequences is much smaller than that of the autocorrelations. As a result, the elements on the main diagonal of the matrix P are much larger than the other elements so that P is with full rank and invertible. Therefore, by solving the linear equation $P\alpha - b = 0$, a group of amplitude estimates can be obtained explicitly as

$$\hat{\alpha} = \begin{bmatrix} \hat{\alpha}_1 \\ \hat{\alpha}_2 \\ \vdots \\ \hat{\alpha}_V \end{bmatrix} = P^{-1}b \tag{4.26}$$

Consequently, with the a priori estimates of the amplitude of the links, the joint timing estimation of V links can be done by solving a convex optimization problem, the result of which can be utilized to refine the amplitude estimation by solving a linear normal equation. Hence, a loop can be built to improve the estimation results to approach similar accuracy as estimating the amplitude and timing simulteneously, which is much more computational consuming. In the case of $V = 1$, Equation (4.26) is simplified to the ratio of the correlation peak to the power of pilots as

$$\hat{\alpha} = \frac{b}{P} = \frac{\sum_{i=0}^{N_{\text{fft}}-1} \Re\big(s(iT_s - \hat{\tau})x^*(iT_s)\big)}{\sum_{i=0}^{N_{\text{fft}}-1} \|s(iT_s - \hat{\tau})\|^2} \tag{4.27}$$

which is exactly the case of independent power estimation.

The performance of the power estimation can be measured by the relative error $\mathcal{J} = \dfrac{\hat{\mathcal{P}} - \mathcal{P}}{\mathcal{P}}$. In the two link case, the performance of the receiver can be evaluated at different positions between the two transmitters as illustrated in Figure 4.5. The comparison of the power estimation of both links with independent and joint method is illustrated in Figure 4.6.

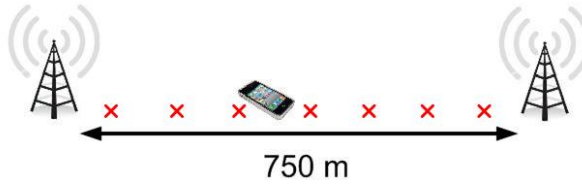

Figure 4.5: Comparison at multiple positions between two transmitters

The horizontal axis in the figure denotes the distance between the mobile station and the first base station, which is set 750[m] away from the other one in the simulation, and the vertical axis $\mathcal{J}$ denotes the relative error of power estimation. It can

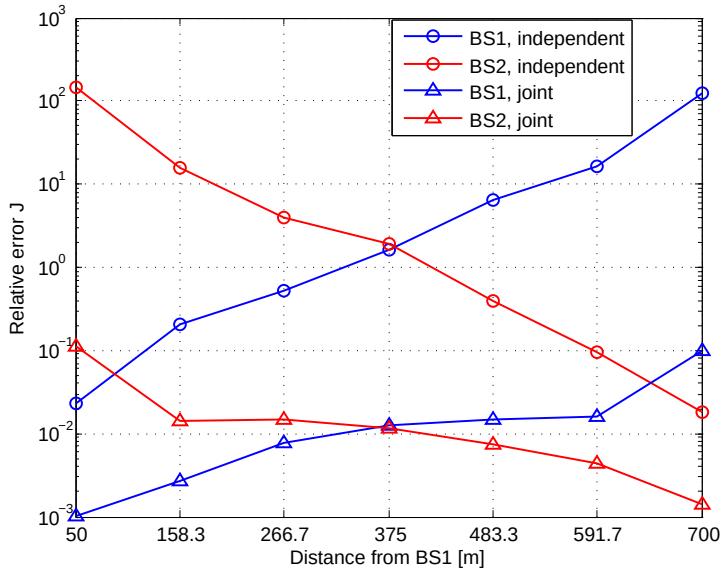

Figure 4.6: Comparison of independent and joint power estimation performance

be seen that by applying joint power estimation, the accuracy of power estimation can be significantly improved compared with estimating each link independently. With more precise power estimation of the received signals, the accuracy of joint synchronization can be further improved, since the target function of optimization in joint timing estimation is dependent on the power of the links as demonstrated in Equation (4.21). Moreover, if the strongest V links have similar power, the sorting of the links according to the independent power estimation can be wrong, which provides the interference cancelation algorithm a non-optimized order of processing. Such problems can be solved by utilizing the joint estimation, since the strong links do not interfere each other in the joint processing.

In the convex optimization algorithms, the computational complexity of the algorithm grows significantly with the increase of the dimension of the search space, so according to feasibility issue we can choose $V = 2$, which can improve the performance for cases with two strong links while without increasing the complexity too much. In such cases, the cost function in timing estimation can be simplified to

$$\begin{aligned} f_\tau(\tau_1,\tau_2) = \sum_{i=0}^{N_{\text{fft}}-1} \Big(&- \hat{\alpha}_1 \Re\big(s_1(iT_s-\tau_1)x^*(iT_s)\big) - \hat{\alpha}_2 \Re\big(s_2(iT_s-\tau_2)x^*(iT_s)\big) \\ &+ \hat{\alpha}_1\hat{\alpha}_2 \Re\big(s_1(iT_s-\tau_1)s_2^*(iT_s-\tau_2)\big)\Big) \end{aligned} \tag{4.28}$$

Similarly, the matrix and vectors in the equation for amplitude estimation are

$$P = \begin{bmatrix} \sum_{i=0}^{N_{\text{fft}}-1} \|s_1(iT_s - \hat{\tau}_1)\|^2 & \sum_{i=0}^{N_{\text{fft}}-1} \Re\big(s_1(iT_s - \hat{\tau}_1)s_2^*(iT_s - \hat{\tau}_2)\big) \\ \sum_{i=0}^{N_{\text{fft}}-1} \Re\big(s_1(iT_s - \hat{\tau}_1)s_2^*(iT_s - \hat{\tau}_2)\big) & \sum_{i=0}^{N_{\text{fft}}-1} \|s_2(iT_s - \hat{\tau}_2)\|^2 \end{bmatrix}$$

$$b = \begin{bmatrix} \sum_{i=0}^{N_{\text{fft}}-1} \Re\big(s_1(iT_s - \hat{\tau}_1)x^*(iT_s)\big) \\ \sum_{i=0}^{N_{\text{fft}}-1} \Re\big(s_2(iT_s - \hat{\tau}_2)x^*(iT_s)\big) \end{bmatrix} \tag{4.29}$$

4.2.2 Joint SIC Method for Multi-link Synchronization

By implementing a maximum-likelihood (ML) estimator, the timing of multiple links can be estimated jointly so that it lowers down the interference level significantly when more than one stations have similar power level. If we combine the joint ML estimator with SIC approach, the parameters of multiple links can be estimated jointly so that the regenerated signal according to the estimates can be subtracted from the original signal, which is more reliable than the independent case used in SIC. As a result, we have a performance gain by introducing a joint SIC method compared with the state-of-the-art independent SIC.

However, due to the raise of computational complexity introduced by the joint estimation for multiple links, it is not efficient to apply the joint estimation all the time, even if we only apply the joint synchronization for $V = 2$ links. If one of the links is dominant, which has much higher power than the second strongest link, the joint estimation of the both links has little gain compared with independent processing. Moreover, in some cases, it should be wisely chosen when the joint estimation should be executed. For example, when there are three main links with power level $\alpha_1^2 \gg \alpha_2^2 > \alpha_3^2$, it is more beneficial to estimate the timing of the strongest station, and jointly synchronize the other two links after canceling the regenerated signal of the strongest link, than to jointly synchronize the strongest two first. Such problems are much more significant when there is interference caused by data and error remains after data decoding, which would be further discussed in Chapter 5.

As a result, we can choose a strategy that monitors both the current strongest link and the second strongest link. By introducing a threshold parameter *thres*, we can judge if the power ratio between the strongest two links exceeds the threshold or not. If the power ratio is no greater than the threshold, i.e. $\alpha_v^2/\alpha_{v+1}^2 \leq thres$, then it indicates that the two links are at the same level of strength so that the v-th and $(v+1)$-th link are synchronized jointly. Otherwise the v-th link can be processed independently. The choice of the parameter *thres* depends on the trade-off between the performance of accuracy and the computational efficiency. When

the requirements of computational time consuming is restricted, the *thres* value should be increased to execute more independent estimation in order to increase the efficiency.

The pseudo-code in Algorithm 1 demonstrates the basic procedures of the joint SIC algorithm for $V = 2$.

Algorithm 1 2-Joint SIC: $\hat{\tau}_{1...K} = \text{JSIC2}(rx, pilot_{1...K}, \alpha_{1...K}, thres)$

Require: $\alpha_1 \geq \alpha_2 \geq ... \geq \alpha_K$
  $v \leftarrow 1$
  $x \leftarrow rx$
  while $v \leq K$ **do**
    if $v = K$ **then**
      $\hat{\tau}_v \leftarrow \text{SYNC}(x, pilot_v)$
      $v \leftarrow v + 1$
    else if $\alpha_v^2/\alpha_{v+1}^2 > thres$ **then**
      $\hat{\tau}_v \leftarrow \text{SYNC}(x, pilot_v)$
      $\hat{x}_v \leftarrow \text{REGENERATE}(pilot_v, \alpha_v, \hat{\tau}_v)$
      $x \leftarrow x - \hat{x}_v$
      $v \leftarrow v + 1$
    else
      $(\hat{\tau}_v, \hat{\tau}_{v+1}) \leftarrow \text{JOINT-SYNC}(x, pilot_v, pilot_{v+1})$
      $\hat{x}_v \leftarrow \text{REGENERATE}(pilot_v, \alpha_v, \hat{\tau}_v)$
      $\hat{x}_{v+1} \leftarrow \text{REGENERATE}(pilot_{v+1}, \alpha_{v+1}, \hat{\tau}_{v+1})$
      $x \leftarrow x - \hat{x}_v - \hat{x}_{v+1}$
      $v \leftarrow v + 2$
    end if
  end while
  return $\hat{\tau}_{1...K}$

4.2.3 Simulation for Multi-link Synchronization using Joint SIC

To test the performance of the joint synchronization method, we start with a two-link model with two base stations 750m separated from each other. The pilots utilized for the synchronization are the primary synchronization sequence (PSS) and the secondary synchronization sequence (SSS). The channel model used in the simulations is the multipath channel in WINNER II [21] including both line-of-sight (LOS) and non-line-of-sight (NLOS) case. In the NLOS scenarios, the time of arrival is estimated based on the first arrived path. We further assume the channel is stationary inside the time interval of one OFDM symbol, and channel estimation is perfect in the simulation, i.e. $\hat{h}(t) = h(t)$. These assumptions hold throughout the following simulations if not stated differently. The impact of the channel is discussed in Chapter 6.

In the simulations, it is assumed that an coarse timing estimation has already been implemented, so that the residual delay is inside the length of cyclic prefix. Under such circumstances, the performance of interference cancelation is shown in Figure 4.7. The simulation scenario is the same as that in Figure 4.3. From the

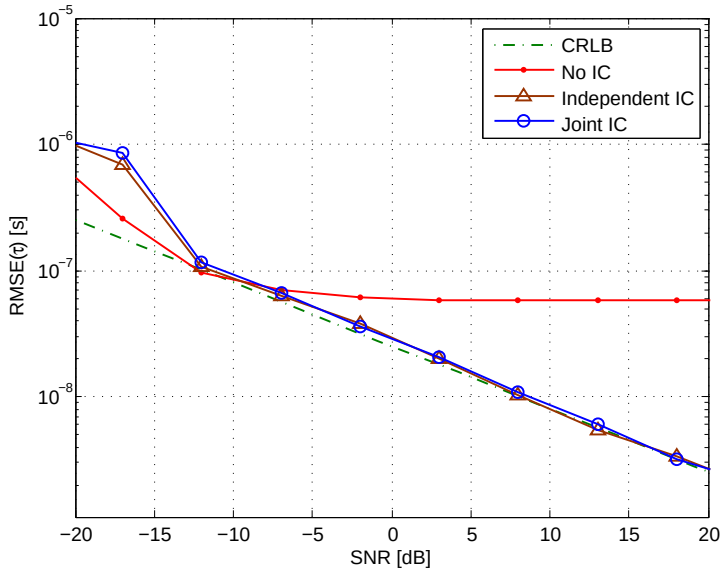

Figure 4.7: Performance comparison of interference cancelation

figure we can conclude that the synchronization accuracy is significantly improved by utilizing interference cancelation methods. The performances between the state-of-the-art SIC approach and the joint SIC algorithm are not distinguishable in such conditions, because the interference is only from the pilot symbols so that it can be correctly subtracted in SIC. If the interference is caused by the data symbols, the performance by SIC degrades due to the propagation of the decoding error for the stronger station, which can be reflected in the simulation results in Chapter 5.

Even for the pilot-caused interference case, an imperfect channel estimation can induct the error propagation effect in SIC, which is shown in Figure 4.8. The curves illustrate the synchronization performance of the link between receivers at different locations and the second base station. In the simulation, the channel estimation is no longer perfect, so the Cramér-Rao lower bound cannot be reached for both interference cancelation methods. The accuracy of imperfect channel estimation is analyzed in Section 6.2. For the right half of the red curve, the second link serves as the stronger link so that the SIC starts from the shown link, the performance of which increases when it is closer to the base station. However, for the locations in the left half of the curve, where the power from the first base station is higher, it can be shown that the independent SIC can no longer achieve the same performance as joint SIC, since the subtracted signal from the stronger link is distorted from the actual signal due to the channel estimation error. The performance degradation is

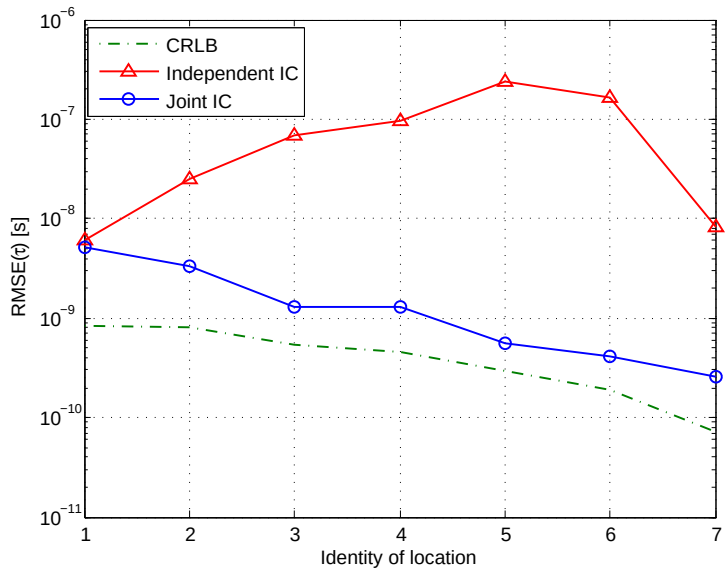

Figure 4.8: Performance of interference cancelation methods at different locations

more apparent at the cell edge, where the power ratio between the stronger link and the weaker link is small, so that the subtracted signal in interference cancelation is distorted more significantly compared with the near station cases.

Chapter 5

Data-caused Inter-cell Interference Cancelation in Multi-link Synchronization

In the communication applications based on OFDM, the tolerance margin of the synchronization error is the difference between the cyclic prefix length and the length of the channel impulse response. There is no inter-symbol interference as long as the timing estimation error is within the range of tolerance. However, for positioning and navigation, it is required to estimate the time of arrival as accurately as possible, since it directly affects the accuracy of the pseudorange. As introduced in Section 2.2.2, in the LTE downlink standard, the PSS and SSS signals are standardized with 1[MHz] bandwidth, which delimitates the Cramér-Rao Lower Bound (CRLB) of the timing estimation. To achieve the high timing precision, additional pilot signal should be utilized besides the synchronization sequences (PSS and SSS) due to their limited bandwidth.

The cell-specific reference signal (CSRS) and the positioning reference signal (PRS) introduced in Section 2.2.3 can be a solution of the problem. The cell-specific reference signal is designed for channel estimation, so it is universal in every frame, and the positioning reference signal is transmitted when the positioning application, which calls for high synchronization accuracy, is provided. Both signals can achieve the maximum bandwidth of 20[MHz], which is much higher than the synchronization sequences. The performance of synchronization with synchronization sequences and positioning reference signal with maximum available bandwidth are compared in Figure 5.1. It can be summarized from the curves that due to the much larger bandwidth, the reference signals can outperform synchronization sequences in both achievable accuracy and convergence speed.

However, the reference sequences are modulated discretely on every other 6 subcarriers of an OFDM symbol. Furthermore, the distribution of the resource elements, on which the reference sequences are modulated, is related to the cell-identity of the transmitter so that the signals from different links may contain the pilots on distinct

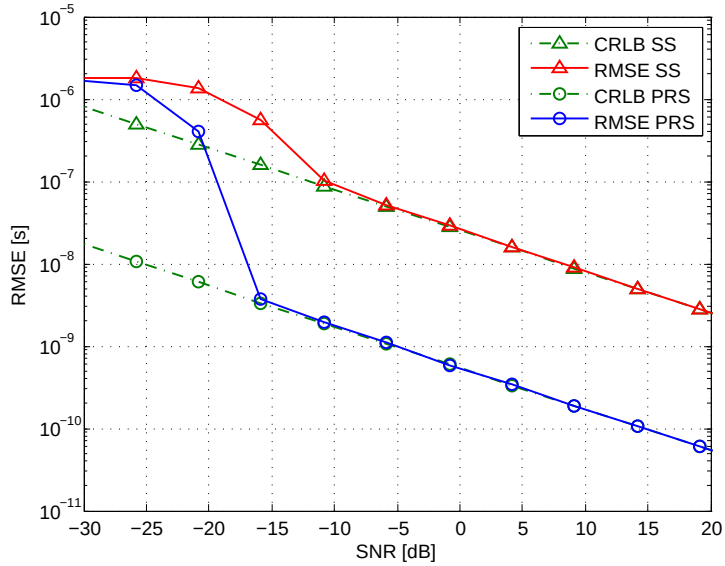

Figure 5.1: CRLB and RMSE comparison between synchronization sequences and positioning reference signal

subcarriers. As a result, the resource elements carrying the reference sequences of one link may be used to transmit data for another link, which results in the inter-cell interference from data.

Different from the pilot-caused interference, the data symbol transmitted are unknown to the receiver so that it cannot be directly regenerated in the interference cancelation. One possible solution for the problem is to estimate the data by deframing, demodulating, and decoding the signal from the strongest link and subtract them altogether with the pilots in the interference cancelation. However, under most circumstances, there is a residual error in the decoded data bits so that the subtracted signal in the interference cancelation might be wrong. In worst case, if the subtracted data symbols are uncorrelated with the actual ones, it even increases the interference power level compared with before interference cancelation. The error can propagate during the process of SIC, which makes the condition even worse.

In this chapter, we derive the relationship between the synchronization performance change after the interference cancelation and the symbol error rate (SER) after decoding. Furthermore, a joint demodulation scheme is combined with the joint SIC method to achieve a better synchronization performance in the condition with data-caused inter-cell interference.

5.1 Performance Estimation of Synchronization with Data-aided Interference Cancelation

In the case with data-caused intercell interference, demodulation and decoding is implemented to mitigate the interference of data signals. If the data symbols are all correctly decoded, the interference is completely canceled when ignoring the error caused by estimation of other parameters. Then the problem is simplified to the condition of pilot-caused interference cancelation, since a correctly decoded data symbol can be treated the same as a known pilot symbol. However, a wrong decoding can degrade the performance of the synchronization. If vector D denotes the data sequence in frequency domain which causes interference, the regenerated sequence $\hat{D}$, which is supposed to be the interference, is subtracted from the signal in interference cancelation. In the worst case, if the subtracted signal sequence $\hat{D}$ is uncorrelated with the actual interference signal sequence D, the new interference power after the subtraction can rise to

$$\mathcal{E}[\|D-\hat{D}\|^2] = \mathcal{E}[\|D\|^2] + \mathcal{E}[\|\hat{D}\|^2] - \mathcal{E}[D^H\hat{D}] - \mathcal{E}[\hat{D}^H D] = 2\mathcal{E}[\|D\|^2] = 2I \quad (5.1)$$

where D^H denotes the Hermitian of the vector D, and we assume the power of the original interfering signal as well as its estimation through decoding are both I, i.e. $\mathcal{E}[\|D\|^2] = \mathcal{E}[\|\hat{D}\|^2] = I$. The second equality in Equation (5.1) holds since the decoded signal is uncorrelated with the actual one under this worst circumstance, so that the mutual information is lowest between the true and the estimated signal.

The Cramér-Rao lower bound (CRLB) indicates the lowest achievable variance of a parameter in the estimation, which bounds the Root Mean Square Error (RMSE) of timing estimation in synchronization process. According to Equation (3.30), CRLB is inversely proportional to the SINR of the signal, and the other terms do not change after subtracting the estimated interference sequences. Therefore, the change of SINR after interference cancelation determines the performance change of synchronization.

Assume the original SINR of the signal from the k-th link can be expressed as

$$\mathrm{SINR}_k = \frac{\mathcal{P}_k}{I+N_k} = \frac{\alpha_k^2}{\sum\limits_{\substack{j\in\{1\ldots K\}\\ j\neq k}} \mathcal{E}[\|D^j\|^2] + \mathcal{E}[\|n_k\|^2]} \quad (5.2)$$

with

$$\mathcal{E}[\|D^j\|^2] = I_j = \alpha_j^2 \quad (5.3)$$

in which $\mathcal{P}_k = \alpha_k^2, I$ and N_k are respectively the power of the signal, the total interference and the complex noise of the k-th link. The noise is assumed to be uncorrelated with neither the signal nor the interference.

If we assume the data sequences from different links are uncorrelated, i.e.

$$\mathcal{E}[(D^k)^H D^j] = 0, \quad (5.4)$$

the change of total interference power after cancelation is simply the superposition of the change of each interferer. This can be shown from

$$\mathcal{E}\Big[\ \big\|\sum_{\substack{j\in\{1\ldots K\}\\ j\neq k}}(D^j-\hat{D}^j)\big\|^2\ \Big]=\sum_{\substack{j\in\{1\ldots K\}\\ j\neq k}}\mathcal{E}\Big[\ \big\|(D^j-\hat{D}^j)\big\|^2\ \Big]. \tag{5.5}$$

Therefore, to simplify the derivation, it is reasonable to assume a two-link case without loss of generality, i.e. the interference is only from one other cell with power $I=\mathcal{E}[\|D\|^2]$.

After one iteration of interference mitigation, the SINR of the processed signal becomes

$$\begin{aligned}\mathrm{SINR}_k^{'}=&\frac{\alpha_k^2}{\mathcal{E}[\|D-\hat{D}+n_k\|^2]}\\ =&\frac{\alpha_k^2}{\mathcal{E}[\|D\|^2]+\mathcal{E}[\|\hat{D}\|^2]+\mathcal{E}[\|n_k\|^2]-2\Re\big(\mathcal{E}[D^H\hat{D}]-\mathcal{E}[D^Hn_k]+\mathcal{E}[\hat{D}^Hn_k]\big)}\\ =&\frac{\alpha_k^2}{2I+N_k-2\Re\big(\mathcal{E}[D^H\hat{D}]\big)}\end{aligned} \tag{5.6}$$

Here we have assumed that the noise vector n_k is uncorrelated with both the interfering data and the its estimation by decoding, i.e. $\mathcal{E}[D^Hn_k]=\mathcal{E}[\hat{D}^Hn_k]=0$. If we denote the i-th data symbol in the length-N sequence D by D_i, it is also reasonable to assume that the sequence $D=\{D_i\},\ i=1,2,\ldots N$ is a pseudo-random sequence that the values of every symbol D_i are chosen independently from the modulation constellation set Q, the size of which is denoted by $|Q|$. Then for arbitrary symbol $a_0\in Q$,

$$p(D_i=a_0)=\frac{1}{|Q|} \tag{5.7}$$

The power of the data sequence, i.e. the interference power, can be expressed as

$$I=\mathcal{E}[\|D\|^2]=\mathcal{E}\Big[\sum_{i=1}^{N}\|D_i\|^2\Big]=\sum_{i=1}^{N}\mathcal{E}[\|D_i\|^2]=N\cdot\frac{1}{|Q|}\sum_{a_0\in Q}\|a_0\|^2 \tag{5.8}$$

According to the definition of the mathemetical expectation,

$$\begin{aligned}\mathcal{E}[\ D^H\hat{D}\ ]=&\sum_{i=1}^{N}\mathcal{E}[\ D_i^*\hat{D}_i\ ]=\sum_{i=1}^{N}\sum_{a_0\in Q}\sum_{a\in Q}a_0^*\cdot a\cdot p(D_i=a_0,\hat{D}_i=a)\\ =&\sum_{i=1}^{N}\Bigg(\sum_{a_0\in Q}\sum_{\substack{a\in Q\\ a\neq a_0}}a_0^*\cdot a\cdot p(D_i=a_0,\hat{D}_i=a,\hat{D}_i\neq a_0)\\ &+\sum_{a_0\in Q}\|a_0\|^2p(D_i=a_0,\hat{D}_i=a_0)\Bigg).\end{aligned} \tag{5.9}$$

For each element of the data sequence,

$$\begin{aligned}\mathcal{E}[D_i^*\hat{D}_i] = &\sum_{a_0\in Q}\sum_{\substack{a\in Q\\ a\neq a_0}} a_0^*\cdot a\cdot p(D_i=a_0,\hat{D}_i=a,\hat{D}_i\neq a_0)\\ &+\sum_{a_0\in Q}\|a_0\|^2 p(D_i=a_0,\hat{D}_i=a_0)\end{aligned} \tag{5.10}$$

Define β as the Symbol Error Rate (SER) of the decoder, i.e. the proportion of the symbols which are mistakenly decoded. It is straightforward that $0\leq\beta\leq 1$. As a result,

$$p(\hat{D}_i\neq a_0|D_i=a_0)=\beta,\quad p(\hat{D}_i=a_0|D_i=a_0)=1-\beta \tag{5.11}$$

By the introduction of β, we can obtain

$$p(\hat{D}_i=a_0,D_i=a_0)=p(\hat{D}_i=a_0|D_i=a_0)\cdot p(D_i=a_0)=\frac{1-\beta}{|Q|} \tag{5.12}$$

If we additionally assume that when a symbol is erroneously decoded, the probabilities of mapping it onto any other symbol are the same, which is reasonable if appropriate channel coding scheme is applied, we can obtain

$$p(\hat{D}_i=a|D_i=a_0,\hat{D}_i\neq a_0)=\frac{1}{|Q|-1} \tag{5.13}$$

As a result, according to the chain rule of conditional probability, it can be derived that

$$\begin{aligned}&p(\hat{D}_i=a,\hat{D}_i\neq a_0|D_i=a_0)\\ =&p(\hat{D}_i=a|D_i=a_0,\hat{D}_i\neq a_0)\cdot p(\hat{D}_i\neq a_0|D_i=a_0)\\ =&\frac{\beta}{|Q|-1}\end{aligned} \tag{5.14}$$

Then we can further obtain that

$$\begin{aligned}&p(D_i=a_0,\hat{D}_i=a,\hat{D}_i\neq a_0)\\ =&p(\hat{D}_i=a,\hat{D}_i\neq a_0|D_i=a_0)\cdot p(D_i=a_0)\\ =&\frac{\beta}{(|Q|-1)|Q|}\end{aligned} \tag{5.15}$$

Therefore, $\mathcal{E}[D_i^*\hat{D}_i]$ can be rewritten as

$$\mathcal{E}[D_i^*\hat{D}_i]=\sum_{a_0\in Q}\sum_{\substack{a\in Q\\ a\neq a_0}} a_0^*\cdot a\cdot\frac{\beta}{(|Q|-1)|Q|}+\sum_{a_0\in Q}\|a_0\|^2\cdot\frac{1-\beta}{|Q|} \tag{5.16}$$

In most cases, the modulation constellation is symmetric, i.e. $\sum_{a_0 \in Q} a_0 = 0$. Consequently, exploiting the symmetry property, we can derive that

$$\sum_{a_0 \in Q} \sum_{a \in Q} a_0^* \cdot a = \sum_{a_0 \in Q} a_0^* \sum_{a \in Q} a = 0 \tag{5.17}$$

$$\sum_{a_0 \in Q} \sum_{\substack{a \in Q \\ a \neq a_0}} a_0^* \cdot a = 0 - \sum_{a_0 \in Q} \|a_0\|^2 = - \sum_{a_0 \in Q} \|a_0\|^2 \tag{5.18}$$

Therefore,

$$\begin{aligned} \mathcal{E}[D_i^* \hat{D}_i] =& \frac{-\beta}{(|Q|-1)|Q|} \sum_{a_0 \in Q} \|a_0\|^2 + \frac{1-\beta}{|Q|} \sum_{a_0 \in Q} \|a_0\|^2 \\ =& \frac{(1-\beta)|Q|-1}{(|Q|-1)|Q|} \cdot \sum_{a_0 \in Q} \|a_0\|^2 \end{aligned} \tag{5.19}$$

$$\begin{aligned} \mathcal{E}[D^H \hat{D}] =& \sum_{i=1}^{N} \mathcal{E}[D_i^* \hat{D}_i] = \sum_{i=1}^{N} \frac{(1-\beta)|Q|-1}{(|Q|-1)|Q|} \cdot \sum_{a_0 \in Q} \|a_0\|^2 \\ =& \frac{(1-\beta)|Q|-1}{|Q|-1} \cdot \underbrace{N \cdot \frac{1}{|Q|} \cdot \sum_{a_0 \in Q} \|a_0\|^2}_{=I} \\ =& \left(1 - \frac{\beta|Q|}{|Q|-1}\right) I \end{aligned} \tag{5.20}$$

Substituting the corresponding term in Equation (5.6) with the result, we can obtain the SINR of the link after interference cancelation as

$$\mathrm{SINR}_k^{'} = \frac{\alpha_k^2}{\frac{2\beta|Q|}{|Q|-1} I + N_k} \tag{5.21}$$

By now, we obtain a formula which describes the relationship between the decoding symbol error rate (SER) β of the interferer and the SINR after interference cancelation processing, which is inversely proportional to the Cramér-Rao lower bound of the timing estimation. It can be verified that when we randomly choose a symbol out of the size-$|Q|$ constellation during the decoding procedure, the symbol error rate is $\beta = (|Q|-1)/|Q|$. As a result, the interference power after processing changes to $2I$ from I according to Equation (5.21), which coincides with the results we derived in Equation (5.1) that the interference power is doubled after the cancelation in the worst case. In contrary, if we have completely correct decoding, i.e. $\beta = 0$, the interference power after cancelation becomes 0 if other errors are ignored. Then it is simplified to the same case as pilot-caused interference cancelation. More

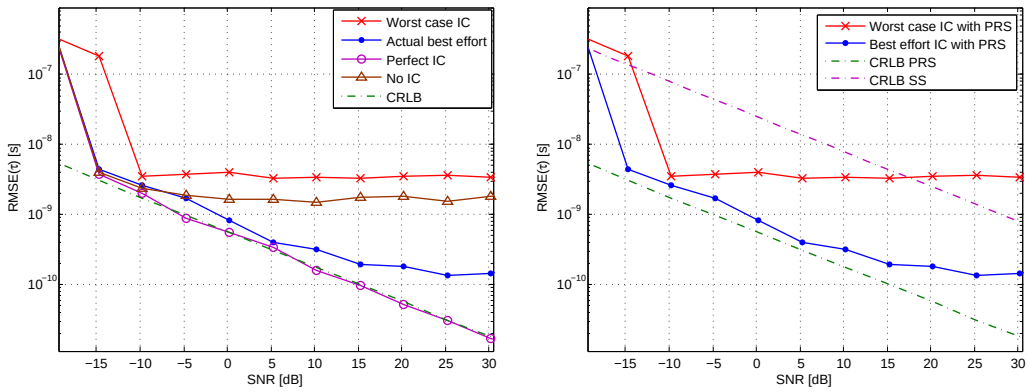

(a) (b)

Figure 5.2: Impact of symbol error rate (SER) on interference cancelation (IC) performance

generally, there is a threshold as $\beta_0 = \frac{|Q|-1}{2|Q|}$. When $\beta < \beta_0$, there is gain in SINR after subtracting the estimated interference, otherwise the performance of synchronization afterwards becomes worse, which may result in vital error propagation in the sequential multi-link interference cancelation.

Figure 5.2(a) illustrates the impact of symbol error rate β in decoding of data-caused interference on the synchronization performance, which is reflected by the root mean square error (RMSE) of the timing estimate of the weaker station in the two-station scenario. The red curve is the performance in the condition that a random generated signal is subtracted in the interference cancelation, which is corresponding to the worst case scenario that $\beta = (|Q| - 1)/|Q|$ and provides an upper bound of the RMSE. It can be observed from the figure that the RMSE is approximately twice as the case without interference cancelation processing, which coincides with the result given by Equation (5.21). The blue curve corresponds to the actual performance of decoding for a mobile terminal 100 meters away from the first base station, the symbol error rate of which is between 0 and $(|Q| - 1)/|Q|$.

Although the performance may degrade if we subtract an incorrectly decoded data sequence, the sense of introducing interference cancelation of data-caused interference can be viewed from Figure 5.2(b). When the SNR is not very high, even in the worst case interference cancelation condition, synchronization with positioning reference signal outperforms the Cramér-Rao lower bound of the synchronization sequences, for which no data-caused interference exists but the bandwidth is much more narrow. The comparison indicates that by introducing interference cancelation for data-caused interference, the synchronization performance is improved compared with timing estimation only with synchronization sequences, although the performance can be degraded due to wrong decoding.

Consequently, on the one hand, we can decide whether to execute the data-aided interference cancelation according to the change of interference power after

cancelation processing. On the other hand, if we obtain an upper bound or estimate of the decoding symbol error rate of the subtracted data, we can also obtain a lower bound or estimate of the RMSE of the synchronization after data-aided interference cancelation.

5.2 Multi-link Joint Synchronization with Joint Demodulation Scheme

In the case that the strongest two links have similar power, the joint SIC method is utilized to achieve a more accurate estimation result. Nevertheless, if data-caused inter-cell interference exists between the two links, the performance will degrade. One possible solution is to decode one of the links and to subtract the decoded data from the signal. However, due to the fact that the two links are with same power level, the demodulation and decoding is significantly affected by the interference from the other link, which may also cause the error propagation problem as discussed in Section 5.1. To cope with the problem, a joint demodulation scheme for the two links can have some gain if the power of the two strongest links are quite close and much stronger than the other links.

To demonstrate the impact of joint demodulation scheme, we assume a two link case and the mobile station locates around the cell edge, i.e. approximately in the middle of the two base stations. The received baseband signal is

$$x(iT_s) = \sum_{k=1}^{2} \alpha_k s_k(iT_s - \tau_k) + n(iT_s) = \sum_{k=1}^{2} \alpha_k (h_k \star d_k)(iT_s - \tau_k) + n(iT_s) \quad (5.22)$$

where $\mathcal{E}[n(iT_s)n^*(iT_s)] = \sigma_N^2$ denotes the noise power, and the large scale fading factor $\alpha_1 > \alpha_2$. In the scenario that more than two links generate interference for the other links, we can simply replace the value of σ_N^2 by σ_{IN}^2 as defined in (4.13).

According to the property of OFDM system, we can rewrite the signal model in frequency domain as

$$\begin{aligned} X(n) &= \sum_{k=1}^{2} \alpha_k S_k(n) \mathrm{e}^{-j2\pi n \Delta f (iT_s - \tau_k)} + N(n) \\ &= \sum_{k=1}^{2} \alpha_k H_k(n) D_k(n) \mathrm{e}^{-j2\pi n \Delta f (iT_s - \tau_k)} + N(n) \end{aligned} \quad (5.23)$$

where $n = -\frac{N_{\text{fft}}}{2}, ..., \frac{N_{\text{fft}}}{2} - 1$, and $N(n)$ is the Gaussian noise on n-th subcarrier after Fourier transform with power $\mathcal{E}[N(n)N^*(n)] = \sigma_N^2$. Under assumption of perfect synchronization and channel estimation, the synchronized and equalized symbol on

n-th subcarrier is

$$\begin{aligned} Y(n) &= \frac{X(n)}{\alpha_1 H_1(n) \mathrm{e}^{-j2\pi n \Delta f (iT_s - \tau_1)}} \\ &= D_1(n) + \frac{\alpha_2 H_2(n)}{\alpha_1 H_1(n)} D_2(n) \mathrm{e}^{-j2\pi n \Delta f (\tau_2 - \tau_1)} + N_Y(n) \end{aligned} \tag{5.24}$$

Consequently, the data symbol of the first link is estimated as one of the symbol in the constellation Q according to

$$\hat{D}_1(n) = \arg\min_{a \in Q} \|Y(n) - a\|^2 \tag{5.25}$$

Due to the influence of different channel parameters and delays from the two links, the data symbol of the weaker link is superposed on the symbol of the stronger link with a phase shift. Without the phase shift, the equalized data symbol never exceeds the decision border of the stronger link in noise free case due to the power difference. However, if the power of both stations are close to each other, the phase shift may make some symbols cross the decision border even without any noise, which results in some demapping error caused by interference. To illustrate the impact, we further assume that the constellations of the data symbols from both stations are QPSK, i.e. $|Q| = 4$, then the equalized signal on all the subcarriers can be plotted in Figure 5.3. The red circles in the figure are the QPSK constellation with the red lines

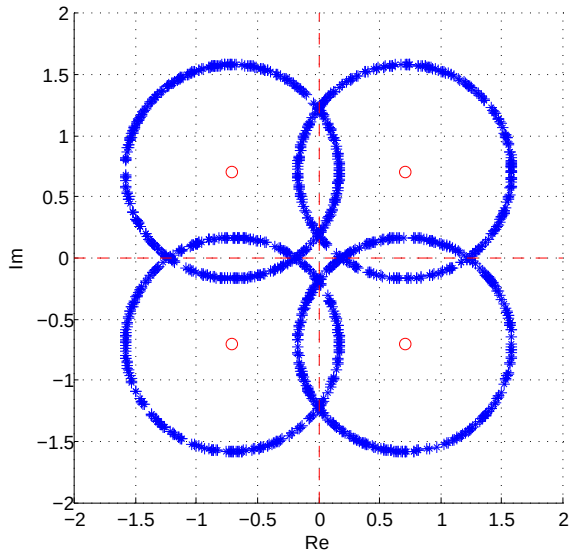

Figure 5.3: Independently equalized symbols

as decision borders, and the blue asterisk are equalized data symbols according to the channel and timing parameter of the stronger station. It can be seen that even in the noise-free condition, there are several symbols beyond the decision border

caused by the interference from the weaker station. If hard decision approach is utilized for demapping, the decoding error of the strongest station propagates in the interference cancelation so that the estimation performance of the weaker station is consequently degraded.

To deal with the demodulation problem at the cell edges, a joint demodulation scheme can be utilized, which demaps strongest two links jointly instead of only equalizing the strongest link. For frequency domain signal on every subcarrier, a new modulation map can be constructed according to the estimated channel and timing parameters of both links, which are assumed to be perfect here. Denoting the constellation of the two jointly estimated links are respectively Q_1 with size $|Q_1|$ and Q_2 with size $|Q_2|$, then we can map the superposition of two symbols $a_v^{(1)} \in Q_1$ and $a_w^{(2)} \in Q_2$ onto a symbol in the new constellation for the n-th subcarrier by

$$\nu_{v,w}(n) = a_v^{(1)}\alpha_1 H_1(n)\mathrm{e}^{-j2\pi n\Delta f(iT_s-\tau_1)} + a_w^{(2)}\alpha_2 H_2(n)\mathrm{e}^{-j2\pi n\Delta f(iT_s-\tau_2)} \tag{5.26}$$

By generating $\nu_{v,w}(n)$ for all the possible symbols in the constellations, i.e. $v = 1, ..., |Q_1|$ and $w = 1, ..., |Q_2|$, we can obtain a size-$|Q_1|\cdot|Q_2|$ new constellation map for the signal on the n-th subcarrier as $Q(n) = \{\nu_{v,w}(n)|v = 1, ..., |Q_1|, w = 1, ..., |Q_2|\}$. In the noise-free case, the received symbol on the n-th subcarrier exactly overlaps with one of the symbols in the new constellation $Q(n)$, if the other parameters of the both links are perfectly estimated. An example of the new constellation map is illustrated in Figure 5.4, in which the minimum distance between two symbols determines the margin of noise tolerance.

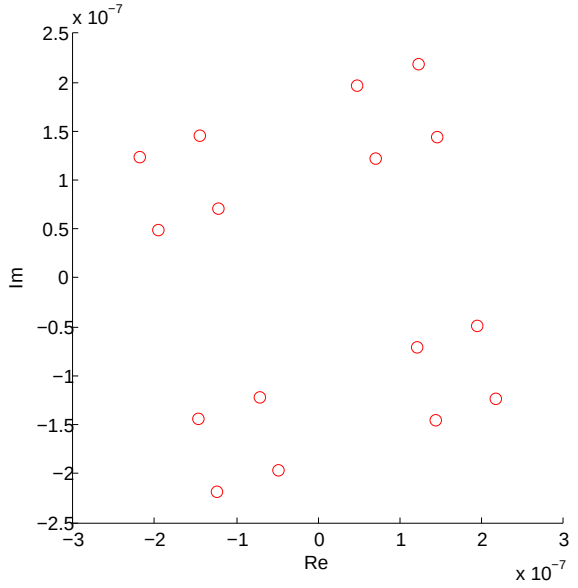

Figure 5.4: An example of joint constellation of two links

The simulation results of the performance of independent demodulation as well

as joint demodulation scheme are compared in Figure 5.5 for two-link cell edge case. The mobile terminal is 350[m] away from the base station 1, and the symbol error rate (SER) in decoding is calculated for various noise level.

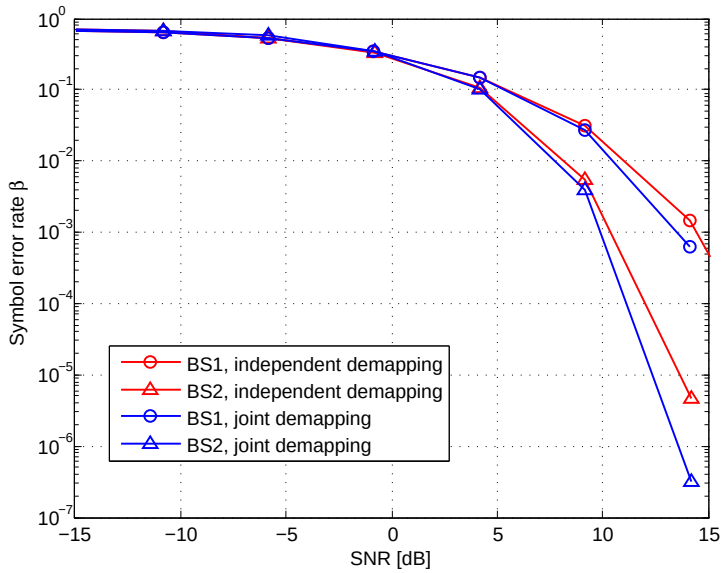

Figure 5.5: Performance comparison of independent and joint demodulation

It can be seen that in such cases, the joint demodulation can achieve better performance, which is measured by symbol error rate (SER). The performance improvement is at the cost of the increased computational complexity. For signals with modulation constellation size $|Q|$, the complexity in demapping by two-link joint demodulation is as $|Q|$-times high as that of independent demodulation. Nevertheless, the computational complexity of both methods are just distinct in a constant multiplication, so the increased complexity by using jointly demapping can be accepted if the application requests for higher accuracy.

5.3 Simulation for Multi-link Synchronization with Data-caused Inter-cell Interference

In the simulation, the 3GPP-LTE positioning reference signal (PRS) as well as the cell-specific reference signal are utilized additional to the synchronization sequences, and the links are chosen with cell identity satisfying that the reference signals from different link are allocated on distinct resource elements, so that each link suffers from the inter-cell interference caused by data of all the other links. Furthermore, no power boost implemented on the pilot symbols, so the pilot symbols have the same power level as data symbols. The other simulation assumptions are the same as in Section 4.2.3.

For the two base station case as illustrated in Figure 4.4, we set a mobile station around the cell edge, and change the transmission power to obtain the performance of multi-link synchronization refers to various SNR, while the power ratio between two base stations are kept as constant, i.e. the signal-to-interference-ratio (SIR) is constant. The root mean square error (RMSE) of timing estimation for both links are shown in Figure 5.6. The curves indicate the three synchronization methods, which

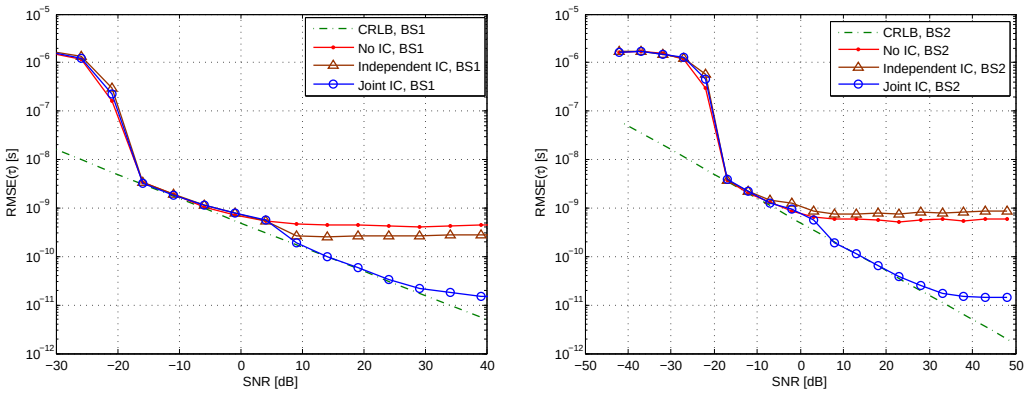

(a) Link with base station 1

(b) Link with base station 2

Figure 5.6: Performance of different synchronization methods for receiver at cell edge in two station case

respectively processes the signal without interference cancelation (IC), with SIC for every link independently, and with SIC for two links jointly. It can be observed that the joint SIC method over performs the other methods. The error of decoding for base station 1 propagates in the independent SIC, so that the performance of synchronization for base station 2 is even worse than the method without interference cancelation.

Furthermore, the performance of synchronization is tested when the receiver is at 15 different locations between the two base stations, as in Figure 4.5. The simulation result is illustrated in Figure 5.7. It is shown that at most locations, both interference cancelation schemes works well compared with synchronization without interference cancelation. However, at the cell edge, when the both links have similar power level, the performance of synchronization utilizing independent SIC degrades due to the decoding error propagation, so that the accuracy is even worse than the case that no interference cancelation is implemented. The problem can be solved by using joint SIC, which outperforms the other two methods at cell edge while has admirable accuracy also at all the other locations.

Therefore, the joint processing method provides intrinsic protection against the strong inter-cell interference when more than one link have equally strong power level, so it outperforms the state-of-the-art SIC approach at the cell edge.

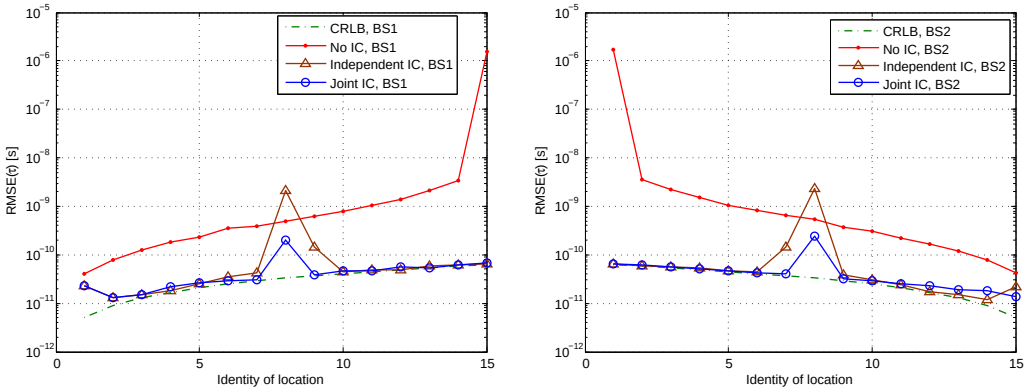

(a) Link with base station 1

(b) Link with base station 2

Figure 5.7: Performance of different synchronization methods at various locations between two stations

Chapter 6

Impact of Multipath Channel

As demonstrated in Section 3.1, Delay locked loops (DLL) can track the timing of the received signal accurately and consistently, and are widely utilized in the fine timing tracking in GNSS and some other systems. However, if the signal is transmitted through a multipath channel, the discriminator output is biased due to the estimation bias in the correlation result of the received signal and the pilot sequence. Nevertheless, in OFDM based system, as shown in Equation (2.8) in Section 2.1, the impact of channel is just multiplication on the signal in frequency domain, which provides the convenience of channel estimation and equalization. Therefore, in OFDM based systems, e.g. LTE, the signal is processed in the baseband, and the impact of multipath can be canceled or mitigated by channel estimation, so that the synchronization result can be more accurate than the biased estimation.

In this chapter, the timing bias caused by multipath in synchronization is estimated, and the state-of-the-art channel estimation approaches are introduced as well as analyzed. Additionally, the simulation results of synchronization with imperfect channel estimation are provided.

6.1 Multipath Bias in Synchronization

For synchronization, the delay τ_0 is usually estimated by correlation. With the presence of multipath in the channel, the estimation is biased if the autocorrelation function is not perfect, which is the actual case. To determine the bias of delay estimation due to the multipath channel, we use the following single link system model:

$$x(t) = \gamma_0 s(t - \tau_0) + \sum_{\iota=1}^{N_L} \gamma_\iota s(t - \tau_0 - \Delta_\iota) + n(t) \tag{6.1}$$

The model represents a signal consisting of one line-of-sight (LOS) path with power $\|\gamma_0\|^2$, and N_L delayed paths with power $\|\gamma_\iota\|^2$ and additional delay Δ_ι for the ι-th path, where γ_0 and γ_ι are complex numbers reflecting the effects of amplitude fading as well as phase shift.

Starting with the simplest case, we assume that there are only two paths including a line-of-sight signal with delay τ_0 and power $\mathcal{P}_{\text{LOS}} = \|\gamma_0\|^2$ along with a multipath signal with power $\mathcal{P}_{\text{MP}} = \|\gamma\|^2$. Therefore, the received signal transmitted over an AWGN channel can be expressed as

$$x(t) = \gamma_0 s(t - \tau_0) + \gamma s(t - \tau_0 - \Delta) + n(t) \tag{6.2}$$

The signal $s(t)$ can be separated into pilot part $s_0(t)$ and data part $d(t)$, which are uncorrelated and fulfill $s(t) = s_0(t) + d(t)$ with $\int_{-\infty}^{+\infty} d(t)s_0^*(t)dt = 0$. Using $R_0(\tau) = \int_{-\infty}^{+\infty} s_0(t)s_0^*(t-\tau)dt$ to denote the autocorrelation function of the reference signal $s_0(t)$, i.e. the pilots part of the signal, the correlation operation at the receiver side can then be denoted as

$$\begin{aligned} R(\tau) &= \int_{-\infty}^{+\infty} x(t)s_0^*(t-\tau)dt \\ &= \int_{-\infty}^{+\infty} (\gamma_0 s(t-\tau_0) + \gamma s(t-\tau_0-\Delta))s_0^*(t-\tau)dt + \int_{-\infty}^{+\infty} n(t)s_0^*(t-\tau)dt \\ &= \int_{-\infty}^{+\infty} \gamma_0 s_0(t-\tau_0)s_0^*(t-\tau)dt + \gamma \int_{-\infty}^{+\infty} s_0(t-\tau_0-\Delta))s_0^*(t-\tau)dt \\ &= \gamma_0 R_0(\tau-\tau_0) + \gamma R_0(\tau-\tau_0-\Delta) \end{aligned} \tag{6.3}$$

The third equality in Equation (6.3) holds for the reason that the noise is uncorrelated with the signal, and the correlation operation does not cause any inter-carrier interference, so the data allocated in the resource elements where the corresponding values in the reference signal are 0 will not affect the correlation result. Assuming a non-coherent correlator which outputs the square of the Euclidean norm of the correlation result, the output will be

$$\begin{aligned} &\psi(\tau) = \|R(\tau)\|^2 \\ =&\left(\gamma_0 R_0(\tau-\tau_0) + \gamma R_0(\tau-\tau_0-\Delta)\right)\left(\gamma_0^* R_0^*(\tau-\tau_0) + \gamma^* R_0^*(\tau-\tau_0-\Delta)\right) \\ =&\|\gamma_0\|^2\|R_0(\tau-\tau_0)\|^2 + \|\gamma\|^2\|R_0(\tau-\tau_0-\Delta)\|^2 \\ &+ 2\Re\big(\gamma_0^*\gamma R_0(\tau-\tau_0-\Delta)R_0^*(\tau-\tau_0)\big) \end{aligned} \tag{6.4}$$

In the case without the second path, i.e. $\gamma = 0$, the maximum of $\psi(\tau)$ appears at $\tau = \tau_0$, which is the actual delay of the LOS signal. However, when $\gamma \neq 0$, the multipath changes the correlation output function $\psi(\hat{\tau})$ as well as where its maximum is achieved at $\hat{\tau} = \arg\max_{\tau} \psi(\tau)$. To determine the bias $\hat{\tau} - \tau_0$, let

$$\psi_0(\tau) = \|R_0(\tau-\tau_0)\|^2, \quad g(\tau) = \Re\big(\gamma_0^*\gamma R_0(\tau-\tau_0-\Delta)R_0^*(\tau-\tau_0)\big) \tag{6.5}$$

Then

$$\psi(\tau) = \|\gamma_0\|^2\psi_0(\tau) + \|\gamma\|^2\psi_0(\tau-\Delta) + 2g(\tau) \tag{6.6}$$

Due to the fact that both $\psi_0(\tau)$ and $g(\tau)$ are real functions, we use a second order Taylor expansion at point τ_0 so that if we omit the higher order terms,

$$\psi_0(\tau) = \psi_0(\tau_0) + \psi_0^{'}(\tau_0)(\tau - \tau_0) + \frac{1}{2}\psi_0^{''}(\tau_0)(\tau - \tau_0)^2 \tag{6.7}$$

$$\psi_0(\tau - \Delta) = \psi_0(\tau_0 - \Delta) + \psi_0^{'}(\tau_0 - \Delta)(\tau - \tau_0) + \frac{1}{2}\psi_0^{''}(\tau_0 - \Delta)(\tau - \tau_0)^2 \tag{6.8}$$

$$g(\tau) = g(\tau_0) + g^{'}(\tau_0)(\tau - \tau_0) + \frac{1}{2}g^{''}(\tau_0)(\tau - \tau_0)^2. \tag{6.9}$$

To find the maximum of the function $\psi(\tau)$, it is required that

$$\begin{aligned} &\frac{d\psi(\tau)}{d\tau} = \|\gamma_0\|^2 \frac{d}{d\tau}\psi_0(\tau) + \|\gamma\|^2 \frac{d}{d\tau}\psi_0(\tau - \Delta) + 2\frac{d}{d\tau}g(\tau) \\ =&\|\gamma_0\|^2\psi_0^{'}(\tau_0) + \|\gamma_0\|^2\psi_0^{''}(\tau_0)(\tau - \tau_0) + \|\gamma\|^2\psi_0^{'}(\tau_0 - \Delta) \\ &+ \|\gamma\|^2\psi_0^{''}(\tau_0 - \Delta)(\tau - \tau_0) + 2g^{'}(\tau_0) + 2g^{''}(\tau_0)(\tau - \tau_0) \\ \stackrel{!}{=}&0 \end{aligned} \tag{6.10}$$

which results in an estimate of the bias

$$\hat{b}_\tau = \hat{\tau} - \tau_0 = -\frac{\|\gamma_0\|^2\psi_0^{'}(\tau_0) + \|\gamma\|^2\psi_0^{'}(\tau_0 - \Delta) + 2g^{'}(\tau_0)}{\|\gamma_0\|^2\psi_0^{''}(\tau_0) + \|\gamma\|^2\psi_0^{''}(\tau_0 - \Delta) + 2g^{''}(\tau_0)} \tag{6.11}$$

According to the definition in Equation (6.5), the value of the bias $\hat{b}_\tau$ only depends on the constant parameter γ and Δ as well as the autocorrelation function of the pilot signal $R_0(\tau)$, but independent on the actual delay of the line-of-sight signal τ_0. Furthermore, the function $\psi_0(\tau) = \|R_0(\tau - \tau_0)\|^2$ achieves its maximum at $\tau = \tau_0$, so $\psi_0^{'}(\tau_0) = 0$.

In more general case, if there are N_L delayed paths besides the LOS path as modeled in Equation (6.1), the correlation function in Equation (6.3) becomes

$$R(\tau) = \int_{-\infty}^{+\infty} x(t)s_0^*(t - \tau)dt = \gamma_0 R_0(\tau - \tau_0) + \sum_{\iota=1}^{N_L} \gamma_\iota R_0(\tau - \tau_0 - \Delta_\iota) \tag{6.12}$$

Similarly as from Equation (6.4) to (6.18), we can apply a non-coherent estimator to calculate $\|R(\tau)\|^2$ and utilize Taylor expansion on each term to obtain an estimate of the multipath bias in similar form of Equation (6.11). Nevertheless, if N_L is high, the formulation of $\|R(\tau)\|^2$ has great amount of cross terms, which results in a complicated expression of the bias.

As a substitutional solution, assuming that the phase information of the LOS signal is demonstrated by $\varphi = \dfrac{\gamma_0}{\|\gamma_0\|}$, if we can obtain the estimation of the phase information $\hat{\varphi}$ by a phase-locked-loop (PLL), a coherent estimator can be constructed as

$$\hat{\tau} = \arg\max_\tau \tilde{\psi}(\tau) = \arg\max_\tau \Re\left(\int_{-\infty}^{+\infty} \hat{\varphi}^* s_0^*(t - \tau)x(t)dt\right) \tag{6.13}$$

According to Equation (6.12), the function $\tilde{\psi}(\tau)$ can be simplified to

$$\begin{aligned}
&\tilde{\psi}(\tau) = \Re\left(\hat{\varphi}^* R(\tau)\right) \\
=&\Re\left(\hat{\varphi}^*\gamma_0 R_0(\tau-\tau_0) + \sum_{\iota=1}^{N_L}\gamma_\iota R_0(\tau-\tau_0-\Delta_\iota)\right) \\
=&\Re\left(\|\gamma_0\| R_0(\tau-\tau_0)\right) + \sum_{\iota=1}^{N_L}\Re\left(\hat{\varphi}^*\gamma_\iota R_0(\tau-\tau_0-\Delta_\iota)\right)
\end{aligned} \tag{6.14}$$

The coherent estimator is non-biased if the received signal is only from the LOS path and the phase estimate is perfect, since $\frac{d}{d\tau}\Re\left(\|\gamma_0\| R_0(\tau-\tau_0)\right)\big|_{\tau=\tau_0} = \|\gamma_0\|\Re\left(R_0^{'}(0)\right) = 0$, where $R^{'}(\tau)$ denotes the first order derivative of the autocorrelation function with respect to τ. However, due to the impact of multipath, the estimated timing $\hat{\tau} = \arg\limits_{\tau}\frac{d}{d\tau}\tilde{\psi}(\tau) = 0$ is biased from the true timing τ_0. If we define

$$\begin{aligned}
g_0(\tau) &= \Re\left(R_0(\tau-\tau_0)\right) \\
g_\iota(\tau) &= \Re\left(\hat{\varphi}^*\gamma_\iota R_0(\tau-\tau_0-\Delta_\iota)\right),
\end{aligned} \tag{6.15}$$

the function $\tilde{\psi}(\tau)$ can be rewritten as the summation of N_L+1 real functions.

$$\tilde{\psi}(\tau) = \|\gamma_0\| g_0(\tau) + \sum_{\iota=1}^{N_L} g_\iota(\tau) \tag{6.16}$$

Implementing second order Taylor expansion at point τ_0 on function $g_\iota(\tau)$ for $\iota = 0, ..., N_L$, we can obtain

$$g_\iota(\tau) = g_\iota(\tau_0) + g_\iota^{'}(\tau_0)(\tau-\tau_0) + \frac{1}{2}g_\iota^{''}(\tau_0)(\tau-\tau_0)^2, \tag{6.17}$$

if the higher order terms are omitted. Thus, the estimated timing $\hat{\tau}$ by the coherent estimator fulfills

$$\begin{aligned}
&\frac{d}{d\tau}\tilde{\psi}(\tau) = \|\gamma_0\|\frac{d}{d\tau}g_0(\tau) + \sum_{\iota=1}^{N_L}\frac{d}{d\tau}g_\iota(\tau) \\
=&\|\gamma_0\|\left(g_0^{'}(\tau_0) + g_0^{''}(\tau_0)(\tau-\tau_0)\right) + \sum_{\iota=1}^{N_L}\left(g_\iota^{'}(\tau_0) + g_\iota^{''}(\tau_0)(\tau-\tau_0)\right) \\
\stackrel{!}{=}&0
\end{aligned} \tag{6.18}$$

Due to the real part of the autocorrelation function R_0 achieves its maximum at 0, i.e. $\Re\left(R_0^{'}(0)\right) = 0$, the term $g_0^{'}(\tau_0) = 0$. Therefore, utilizing a coherent estimator,

the total bias of correlation-based timing estimation caused by N_L multipaths is approximately

$$\hat{b}_\tau = \hat{\tau} - \tau_0 = -\frac{\sum_{\iota=1}^{N_L} g_\iota^{'}(\tau_0)}{\|\gamma_0\| g_0^{''}(\tau_0)(\tau - \tau_0) + \sum_{\iota=1}^{N_L} g_\iota^{''}(\tau_0)(\tau - \tau_0)} \tag{6.19}$$

As a result, as long as the power, delay, and phase shift of all the multipath signals are reliably estimated, the bias of correlation-based timing estimation result caused by multipath channel can be estimated by Equation (6.19). However, from the feasibility and complexity point of view, it is quite difficult to obtain the reliable estimates of such parameters, so channel estimation in frequency domain with help of the property of OFDM system is implemented in most practical conditions instead.

6.2 Channel Estimation in OFDM

For the reason that the impact of multipath channel in OFDM system is multiplied on the frequency domain signals, the channel response influencing on the n-th subcarrier of the l-th OFDM symbol can be simply treated the same as the value of a transfer function $H(l, n)$. As a result, the estimation of the channel impulse response can be substituted by the problem of estimating the transfer function with discrete stochastic entries. Aided by the designed pilots $S_0(l, n)$, the received signal is

$$S(l, n) = H(l, n)(S_0(l, n) + D(l, n)) + N(l, n) \tag{6.20}$$

On the resource elements $\Omega = \{(l^{'}, n^{'})\}$ locate the pilot symbols, $D(l^{'}, n^{'}) = 0$, otherwise the resource element is seized by data symbol, i.e. $S_0(l, n) = 0$, if $(l, n) \notin \Omega$.

P. Hoeher, S. Kaiser, and P. Robertson proposed a 2-D Wiener filter approach in [22, 23], which builds a 2-D filter with impulse response that minimizes the mean square error (MSE) of the estimation, i.e.

$$\hat{\omega}_{l,n} = \arg\min_{\omega_{l,n}} \mathcal{E}[\ \|H(l, n) - \hat{H}(l, n)\|^2\ ] \tag{6.21}$$

where the estimation of the channel impact on resource element (l, n) is obtained by the interpolation of the estimated channel parameters of pilots

$$\hat{H}(l, n) = \sum_{(l^{'}, n^{'}) \in \Omega} \omega_{l,n}(l^{'}, n^{'}) \tilde{H}(l', n') \tag{6.22}$$

in which

$$\tilde{H}(l', n') = \frac{S(l^{'}, n^{'})}{S_0(l^{'}, n^{'})} = H(l^{'}, n^{'}) + \frac{N(l^{'}, n^{'})}{S_0(l^{'}, n^{'})} \tag{6.23}$$

The tap number of the 2-D Wiener filter is the number of pilot symbols $|\Omega|$. The performance of the 2-D Wiener filter approach measured by MSE of the transfer function value $H(l, n)$ is given in Figure 6.1

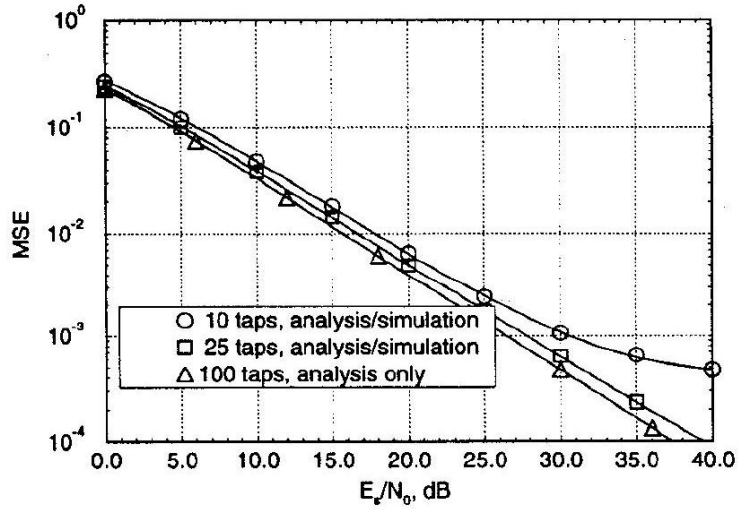

Figure 6.1: Average MSE versus SNR for 2-D Wiener filtering given a rectangular grid [22]

Y. Li et al. proposed an MMSE channel estimator [24] which utilize the correlation of the frequency response of dispersive fading channels and verified to be robust to model mismatch between the channel and the estimator. B.H. Fleury et al. proposed another state-of-the-art channel estimation method [25] based on SAGE algorithm [26], which jointly estimates the parameters of multiple paths to obtain the channel response. The SAGE based method can achieve outstanding performance but the computational complexity is also much higher compared with the other state-of-the-art approaches.

For all the simulations in which the multipath channel impacts are considered, we generate the channel utilizing WINNER II multipath channel model. Both the line-of-sight (LOS) and non-line-of-sight (NLOS) conditions are introduced according to the line of sight probability modeled in [21] that in urban area

$$p_{\mathrm{LOS}} = \min(\frac{18}{d}, 1) \cdot (1 - \mathrm{e}^{-\frac{d}{63}}) + \mathrm{e}^{-\frac{d}{63}} \tag{6.24}$$

where d is the distance from the transmitter to the receiver in unit of meter.

On the receiver side, an artificial Gaussian noise is added on the actual channel impulse response to model the channel estimation error, i.e. the channel estimation result is assumed to be the perfect estimation plus a noise. The power of the noise is set according to the MSE curve provided in Figure 6.1, which illustrates the channel estimation performance of the state-of-the-art 2-D Wiener approach.

It should be mentioned that the performance in Figure 6.1 is obtained utilizing pilot pattern with spacing of 3 time samples in time domain and 6 subcarriers in frequency domain. Compared with the cell-specific reference signals in LTE downlink as shown in Figure 2.3, the pilots in [22, 23] are allocated slightly denser in time domain, which results in higher estimation accuracy. Therefore, it is only an approximation of the channel estimation result by adding a Gaussian noise with power according to curves in Figure 6.1, and the approximation is slightly optimistic due to the curves are obtained by utilizing a denser pilot pattern.

The impact of multipath as well as channel estimation on the synchronization performance in single link case is illustrated in Figure 6.2, in which the vertical axis is the RMSE of synchronization using synchronization sequences (PSS and SSS). The

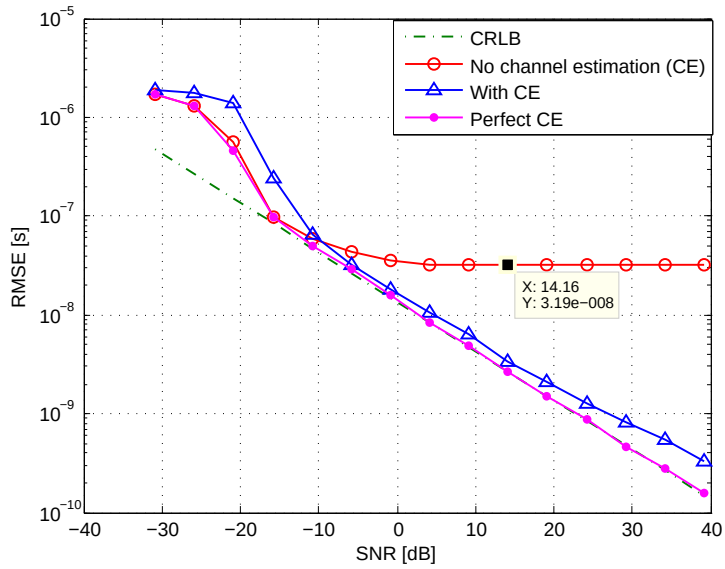

Figure 6.2: Bias in synchronization caused by channel and the performance of channel estimation

impact of multipath channel on synchronization can be reflected by the saturation of the curve without channel estimation. The multipath bias in synchronization calculated by Equation (6.19) is 3.21×10^{-8}[s], which is close to the actual bias in simulation, indicating the approximate estimation is reasonable. The other two curves reflect the performance of the channel estimation. With perfect channel estimation, the impact of channel can be almost canceled so that the curve can reach the Cramér-Rao lower bound in high SNR region. If the channel estimation is imperfect, which is the actual case in practice, the performance of synchronization is affected by the channel so that it cannot reach the bound. Nevertheless, it can be observed that the influence of multipath is significantly mitigated, and the bias declines when SNR increases due to the decrease of channel estimation error.

Chapter 7

Positioning with High Accuracy Timing

In modern GNSS systems, the position of the user is resolved utilizing the measurements of pseudorange and carrier phase. However, in the positioning service based on wireless communication systems such as LTE, the carrier phase measurements are unreliable because of inaccurate clock and oscillator with relatively high level of phase noise. Compared with GNSS systems, the non-line-of-sight scenarios as well as stronger multipath and interference make the problem more severe in ground based positioning. As a result, the communication system based positioning uses only pseudorange measurements which is the time of arrival (ToA) measurements multiplied by the speed of light. For a certain receiver, the pseudorange of the k-th link is

$$\rho^k = c\hat{\tau}_k, \quad c \approx 2.998 \times 10^8 \text{m/s} \tag{7.1}$$

Due to the time of arrival is scaled by the large number of speed of light, the accuracy of pseudorange measurement is extremely sensitive to the error of timing estimation in synchronization. An error of 1 ns in ToA measurement results in 30 cm error in pseudorange, which is non-negligible in some positioning and navigation services. Therefore, high accuracy synchronization is essential in positioning application.

In this chapter, the range based positioning algorithm is introduced firstly, and the proposed high accuracy multi-link synchronization scheme is applied to obtain precise positioning result over the whole cellular network, the simulation outcomes of which are also provided.

7.1 Range-based Positioning Algorithm

In modern positioning and navigation systems, the position of a user is calculated according to the range, i.e. the straight distance, between the user several satellites or ground stations with known position. In practice, the range is measured by multiplying speed of light and the time of arrival obtained through synchronization,

which is noisy. Consequently, the measurement of range is actually noisy, which is called pseudorange. As introduced in [27], denoting the pseudorange of the k-th link as ρ^k, the position of satellites or ground stations as $\vec{r}^{\,k}$ with $k = 1, ..., K$, and the position of the user as $\vec{r} = (x, y, z)^T$. Then the pseudorange of the k-th link can be simply expressed as

$$\rho^k = \|\vec{r} - \vec{r}^{\,k}\| + c(\delta - \delta^k) + \eta^k \tag{7.2}$$

where δ and δ^k denotes the clock offset of the receiver and the k-th transmitter perspectively, and the noise of the k-th pseudorange measurement is denoted by η^k with power $\mathcal{E}[\ \eta^k \eta^{k^*}\ ] = (\sigma_\eta^2)^{(k)}$. According to the relation between the pseudorange and the estimated time of arrival demonstrated in Equation (7.1), the residual error in timing estimation affects the pseudorange measurement by

$$\rho^k = c\hat{\tau}_k = c(\tau_k + \delta - \delta^k + n_k) \tag{7.3}$$

in which n_k is the equivalent noise of k-th ToA estimation with variance $\mathcal{E}[\ n_k n_k^*\ ] = (\sigma_\tau^2)^{(k)}$, which equals to the mean square error(MSE) of the timing estimation in clock-offset-free case. Then the noise of pseudorange measurement can be expressed as

$$(\sigma_\eta^2)^{(k)} = \mathcal{E}[\ \eta^k \eta^{k^*}\ ] = \mathcal{E}[\ c^2 n_k n_k^*\ ] = c^2 (\sigma_\tau^2)^{(k)} \tag{7.4}$$

By introducing the unit vector $\vec{e}^{\,k} = \dfrac{\vec{r} - \vec{r}^{\,k}}{\|\vec{r} - \vec{r}^{\,k}\|}$, the true range can be denoted by $\|\vec{r} - \vec{r}^{\,k}\| = (\vec{e}^{\,k})^T(\vec{r} - \vec{r}^{\,k})$, so that the pseudorange measurement equation (7.2) of all K links can be demonstrated in vector and matrix form as

$$\rho = H \begin{bmatrix} \vec{r} \\ c\delta \end{bmatrix} + \eta \tag{7.5}$$

in which H is redefined as the geometry matrix, and the vectors and matrices are defined as

$$\rho = \begin{bmatrix} \rho^1 + (\vec{e}^{\,1})^T \vec{r}^{\,1} + c\delta^1 \\ \rho^2 + (\vec{e}^{\,2})^T \vec{r}^{\,2} + c\delta^2 \\ \vdots \\ \rho^K + (\vec{e}^{\,K})^T \vec{r}^{\,K} + c\delta^K \end{bmatrix}, \quad H = \begin{bmatrix} (\vec{e}^{\,1})^T, 1 \\ (\vec{e}^{\,2})^T, 1 \\ \vdots \\ (\vec{e}^{\,K})^T, 1 \end{bmatrix}, \quad \eta = \begin{bmatrix} \eta^1 \\ \eta^2 \\ \vdots \\ \eta^K \end{bmatrix} \tag{7.6}$$

As a result, the positioning problem has been transferred into a linear normal equation containing 4 unknowns. If we have a priori information of the noise variance of all the links, the overall noise power should be weighted, in order to achieve fairness for all the links according to their reliability information. The weighting matrix can be constructed as

$$W = \Sigma^{-1} = \begin{bmatrix} (\sigma_\eta^2)^{(1)} & & & \\ & (\sigma_\eta^2)^{(2)} & & \\ & & \ddots & \\ & & & (\sigma_\eta^2)^{(K)} \end{bmatrix} \tag{7.7}$$

Then if $K \geq 4$, the least square solution of Equation (7.5) should be

$$\begin{bmatrix} \hat{\vec{r}} \\ c\hat{\delta} \end{bmatrix} = \arg\min_{\vec{r},\delta} \|\eta^T \eta\|_W^2 = (H^T W H)^{-1} H^T W \rho \tag{7.8}$$

which provides the solution of the user's position and clock offset. However, in the expression of solution, the matrix H is related with the unknown position $\vec{r}$. By utilizing numeric iterative algorithm, the H matrix can be obtained iteratively. Using a guess of $\vec{r}$ as initialization, e.g. $\vec{r}^{(0)} = [0, 0, 0]^T$, the position can be calculated iteratively by

$$\begin{aligned} \begin{bmatrix} \hat{\vec{r}}^{(q+1)} \\ c\hat{\delta} \end{bmatrix} &= ({H^{(q)}}^T W H^{(q)})^{-1} {H^{(q)}}^T W \rho \\ H^{(q+1)} &= \begin{bmatrix} \dfrac{(\vec{r}^{(q+1)} - \vec{r}^{1})^T}{\|\vec{r}^{(q+1)} - \vec{r}^{1}\|}, & 1 \\ \vdots & \\ \dfrac{(\vec{r}^{(q+1)} - \vec{r}^{K})^T}{\|\vec{r}^{(q+1)} - \vec{r}^{K}\|}, & 1 \end{bmatrix} \end{aligned} \tag{7.9}$$

It can be shown that with the linearization and iteration by inducting unit vector $\vec{e}$, the iterative least square solution of the linear equation is equivalent to the solution of first order Newton iterative method. Consequently, the position of the user can be obtained according to time of arrival measurements from multiple links.

In communication system based positioning, the situation varies significantly from GNSS system. First of all, the transmitters are on the ground stations instead of satellites, which results in a poor transmitter constellation in vertical dimension of the local coordinates due to the similar height of all stations as well as the receiver. As a result, the positioning result of z is rather unreliable so that it is abandoned under many circumstances, because the users are not interested in the height information in most communication system based positioning applications. Moreover, the convergence of the Newton iterative method is slower compared with positioning with GNSS, because the initialization of the position has a much stronger impact on the unit geometry vector $\vec{e}^k$.

In addition, the signals propagate near the ground without passing through the atmosphere, so the atmosphere impact, e.g. ionospheric as well as tropospheric delay, can be ignored, which results in the simplified system model in Equation (7.2). Nevertheless, compared with GNSS system, the multipath effect and inter-cell interference is much stronger, which are the main concerns of Chapter 4, 5 and 6.

More vitally, the atomic clocks in GNSS transmitters are not implemented in transmitters in base stations, which causes the unsynchronized clock among all the transmitters. Consequently, the clock offset δ^k is actually unknown and assumed to be 0 in calculation, which degrades the accuracy of positioning. Moreover, the

clock offset of the receiver δ is unnecessary to be estimated if δ^k is not provided. Nonetheless, the offset of the receiver clock is much more urgent than transmitter clock offset for the reason that the base stations are roughly synchronized in clock but may have significant clock offset with the receiver. To remove the impact of the receiver clock, the time difference of arrival (TDoA) is measured instead of ToA, which is a similar scheme similar as using double difference navigation signal to remove receiver bias. By selecting a link as the fundament, TDoA is obtained by calculating the difference between the ToA of the k-th link and the fundamental link, so that the following equation holds if we ignore the clock difference among the transmitters.

$$\rho^{k1} = c(\tau_k - \tau_1) = \rho^k - \rho^1 = (\vec{e}^{k1})^T \vec{r} - (\vec{e}^{k})^T \vec{r}^k + (\vec{e}^{1})^T \vec{r}^1 + \eta^{k1} \tag{7.10}$$

where $\vec{e}^{k1} = \vec{e}^k - \vec{e}^1$ is the unit vector pointed from the k-th transmitter to the first transmitter, δ^{k1}, and $\eta^{k1} = \eta^k - \eta^1$. It can be observed that the clock offset of the receiver is canceled by utilizing TDoA measurements.

7.2 Simulation for Positioning in LTE

Calculating the differential pseudorange by TDoA measurements can remove the impact of receiver clock offset. As an approximate simplification, ToA measurements are utilized to calculate the pseudorange in the simulation, while the receiver clock offset is set to 0. Furthermore, the base stations are assumed to be perfectly synchronized, which leads to an optimistic result. Nevertheless, if the base stations have line-of-sight with GNSS satellites, the synchronization error among different base stations is not critical. The ToA is estimated by synchronization utilizing all the four sorts of pilots standardized in LTE downlink as introduced in Section 2.2. The positioning error is calculated with the root mean square error (RMSE) in $x-y$ dimensions, because the geometry of the height dimension z is poor in ground station based positioning, and the users only concern their 2-D position in most ground station based navigation applications. Nevertheless, the height difference of the transmitters on base stations and the receiver antenna is considered in the iterative calculation of the receiver position. In addition, three multi-link synchronization methods are implemented to obtain the ToA measurements, the performances of which can be compared by the RMSE of positioning. The first synchronization method regards all the links independently while no interference cancelation scheme is implemented, and the second approach utilizes the state-of-the-art multi-link detection method which executes successive interference cancelation (SIC). Instead of synchronizing and subtracting each link independently and successively, the third method utilizes the joint SIC scheme proposed in Chapter 4 as well as the joint demodulation scheme proposed in Chapter 5, which processes the strongest two links simultaneously when the power of them are close to each other. In the latter two methods with interference cancelation, parallel interference cancelation (PIC) is im-

plemented after obtaining a group of a priori estimation of parameters from all the links, either by independent SIC or joint SIC.

The performance of the positioning is simulated when the mobile station locates at different positions of the cell. We use a three base station model as in Figure 7.1, in which the three base stations are labeled by identity 1 to 3. According to the symmetry of the cellular network, the three routes in Figure 7.1 are typical to represent most possible conditions of the receiver's location. In the simulation, 15 locations are chosen on each route, which are uniformly distributed on the route. The 15 locations are labeled by identities from 1 to 15, in which the position closest to the upper-left base station is labeled by 1 and the farthest has identity 15 for all three routes. The antenna pattern of the base stations are considered, so the power field of all three stations are shown in Figure 7.2. According to the power map, the power condition of all the links can be looked up for all the locations in Figure 7.1.

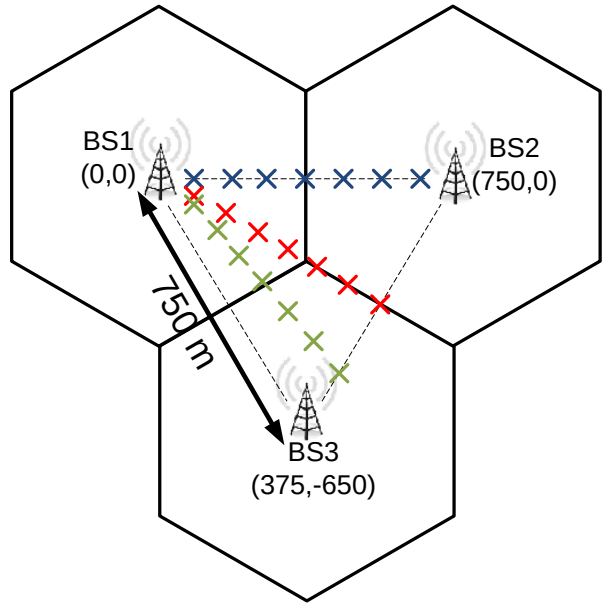

Figure 7.1: Routes covering typical locations

For the blue route between the upper two base stations, the performance of positioning applying the multi-link synchronization methods is illustrated in Figure 7.3. It can be observed from the simulation result that the positioning performance of the first intuitive method is poor when the receiver is close to the base stations, since the signals from the weaker links are drowning in the signal of the strongest link. The problem can be solved by applying independent interference cancelation (IC), which has excellent performance when the subtracted link has very high SINR. However, at the location number 1, which is closest to the serving base station, the performance of independent IC is limited. The reason for the performance degradation is that although one link has dominant power, the other two weaker links have similar power

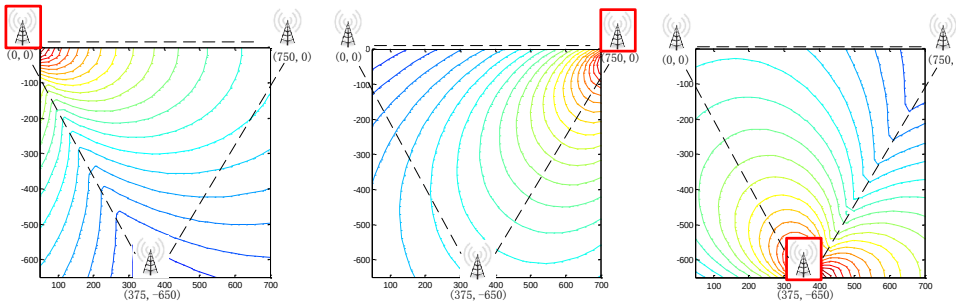

(a) Power field of 1st link (b) Power field of 2nd link (c) Power field of 3rd link

Figure 7.2: Power impact map of each link

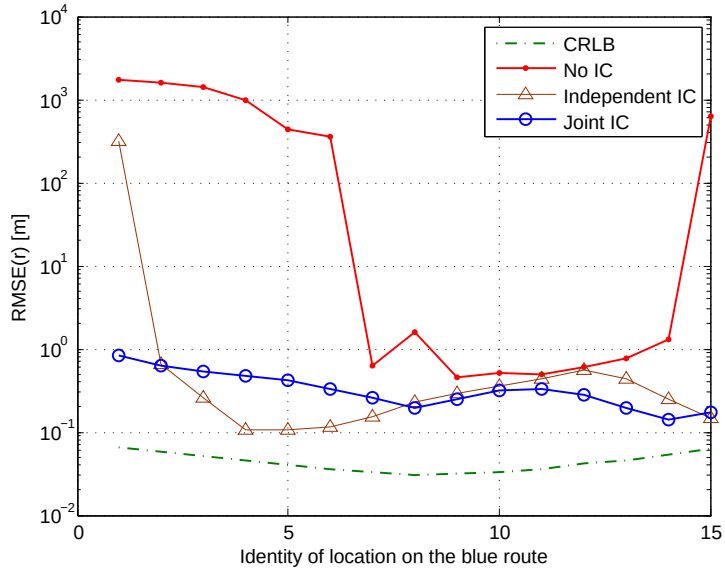

Figure 7.3: Performance of positioning for mobile stations on the blue route

level, which can be indicated from the power map in Figure 7.2, so that in the second step of SIC, the estimated link suffers from strong interference caused by the last link. Compared with the other two methods, positioning with pseudorange measurements utilizing joint SIC in synchronization has best performance for most locations, and the error is bounded at all locations. The similar conclusion can be achieved for the other two routes, the positioning performances of which are illustrated in Figure 7.4 and 7.5.

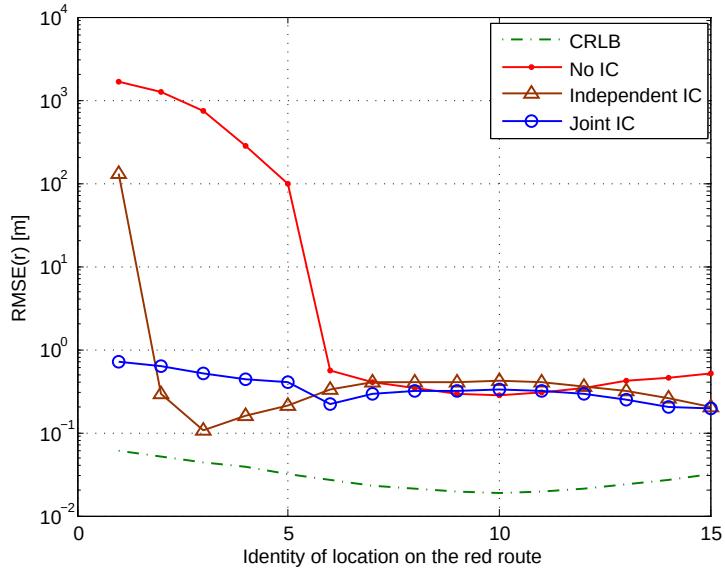

Figure 7.4: Performance of positioning for mobile stations on the red route

Therefore, we can deduce that by applying the joint SIC as well as joint demodulation in synchronization, the positioning error remains low all over the cell area due to the high accuracy timing estimation for all three links. In the simulation condition, at all the locations, the positioning error by joint synchronization method is below 1 [m], which can fulfill the demands from most of the applications in ground station based navigation.

It should be mentioned that the simulation results are based on the optimistic assumption that the base stations are perfectly synchronized and the non-line-of-sight delay is ignored. However, if the base stations have line-of-sight connection with GNSS satellites, the timing can be obtained precisely so that the synchronization error among different base stations is limited. In addition, the impact of NLOS can be mitigated if the non-line-of-sight detection technique is implemented as introduced by C. Gentner and S. Sand in [28]. Therefore, by applying appropriate techniques to mitigate the performance degradation when the assumptions are violated, the simulation results remain reliable.

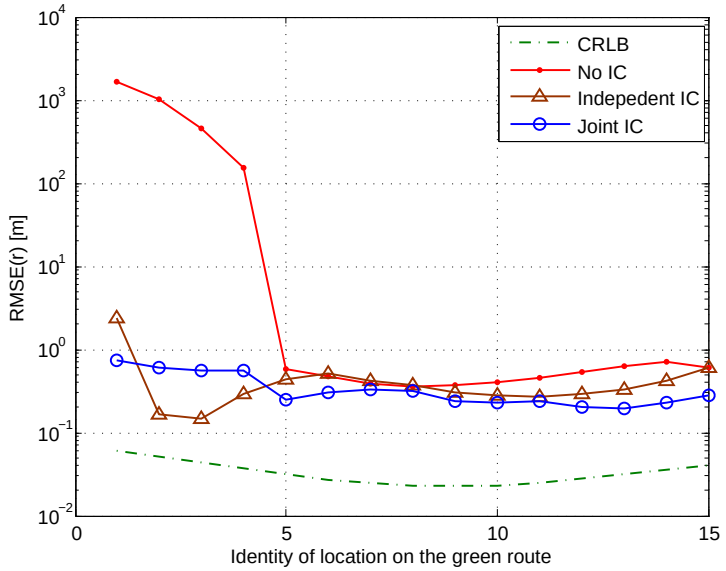

Figure 7.5: Performance of positioning for mobile stations on the green route

Chapter 8

Conclusion

In this work, multi-link synchronization for 3GPP-LTE downlink is concerned. To achieve sub-sample accuracy to satisfy the requirement of positioning and navigation, frequency domain correlation and interference cancelation scheme are implemented and analyzed.

For the multi-link case with interference caused by pilots, a maximum-likelihood joint timing estimator is proposed to process a few links simultaneously so that the interference among the co-processed links can be removed. The approach is verified to be able to achieve the Cramér-Rao lower bound of timing estimation for all the jointly processed links. In addition, the power of all the links can be estimated jointly when the timing is estimated. The joint power estimation is approved to significantly outperform the independent power estimation for all the links.

Besides the pilot-caused interference, the synchronization in LTE downlink can also be interfered by data symbols of other cells. As a result, a decoding procedure should be added into the interference cancelation. Depending on the decoding symbol error rate, the synchronization performance after subtracting the decoded signal in interference cancelation can be better or worse. An explicit form of the relation between the SINR after data-aided interference cancelation and the decoding symbol error rate is derived in this work.

Furthermore, a joint demodulation scheme in OFDM is proposed to reduce the symbol error rate when there exists two links with similar power level, which is the case when a receiver is at the cell edges. Based on the joint schemes for synchronization, power estimation and demodulation, a joint successive interference cancelation (joint-SIC) algorithm is proposed. The joint-SIC algorithm measures the power ratio between the strongest two links in every stage, and processes the two links jointly when they have similar power level while only the strongest link is handled otherwise. By successively subtracting the regeneration of the signal from processed links, the interference can be canceled. It is approved that the joint-SIC has much better performance compared with the state-of-the-art SIC approach when multiple links have similar power, which is the ordinary case at the cell edges of a cellular network.

The proposed interference cancelation algorithm has been utilized to achieve

high precision timing, so that it can be applied in range-based positioning. The performance of the positioning has been simulated at various locations spreading over a whole cell. According to the simulation result, the positioning error by utilizing joint-SIC algorithm remains low in the whole cell, which outperforms the SIC approach and the method without interference cancelation.

In the future work, the channel impact becomes the vital problem in LTE based positioning. First of all, the channel estimation is to be implemented, which is approximated by utilizing the results of the state-of-the-art approaches in this work. In addition, the non-line-of-sight signal introduces extra delay in the ToA measurements, which makes the pseudorange measurements biased from the true range. The extra delay can be dominant compared with the synchronization error by utilizing high precision joint estimation. As a result, to detect the non-line-of-sight signals and remove their degradation impacts on performance is an interesting topic. Moreover, the carrier frequency offset is assumed to be completely removed in this work. The frequency offset is usually estimated simultaneously with the timing acquisition and corrected before the fine timing estimation. However, the estimation and correction cannot be perfect in practice. Therefore, the proposed high precision synchronization method should be improved to be more robust to carrier frequency offset.

Bibliography

[1] M. Morelli, C.-C. Kuo, and M.-O. Pun, "Synchronization techniques for orthogonal frequency division multiple access (ofdma): A tutorial review," *Proceedings of the IEEE*, vol. 95, pp. 1394 –1427, July 2007.

[2] T. Schmidl and D. Cox, "Robust frequency and timing synchronization for ofdm," *Communications, IEEE Transactions on*, vol. 45, pp. 1613 –1621, Dec 1997.

[3] H. Minn, V. Bhargava, and K. Letaief, "A robust timing and frequency synchronization for ofdm systems," *Wireless Communications, IEEE Transactions on*, vol. 2, pp. 822 – 839, July 2003.

[4] K. Shi and E. Serpedin, "Coarse frame and carrier synchronization of ofdm systems: a new metric and comparison," *Wireless Communications, IEEE Transactions on*, vol. 3, pp. 1271 – 1284, July 2004.

[5] J. van de Beek, M. Sandell, and P. Borjesson, "Ml estimation of time and frequency offset in ofdm systems," *Signal Processing, IEEE Transactions on*, vol. 45, pp. 1800 –1805, July 1997.

[6] F. Berggren and B. Popovic, "A non-hierarchical cell search scheme," in *Wireless Communications and Networking Conference, 2007.WCNC 2007. IEEE*, pp. 2300 –2304, March 2007.

[7] G. Boudreau, J. Panicker, N. Guo, R. Chang, N. Wang, and S. Vrzic, "Interference coordination and cancellation for 4g networks," *Communications Magazine, IEEE*, vol. 47, pp. 74 –81, April 2009.

[8] J. Andrews, W. Choi, and R. Heath, "Overcoming interference in spatial multiplexing mimo cellular networks," *Wireless Communications, IEEE*, vol. 14, pp. 95 –104, December 2007.

[9] P. Patel and J. Holtzman, "Analysis of a simple successive interference cancellation scheme in a ds/cdma system," *Selected Areas in Communications, IEEE Journal on*, vol. 12, pp. 796 –807, June 1994.

[10] M. Varanasi and B. Aazhang, "Multistage detection in asynchronous code-division multiple-access communications," *Communications, IEEE Transactions on*, vol. 38, pp. 509 –519, Apr 1990.

[11] D. Divsalar, M. Simon, and D. Raphaeli, "Improved parallel interference cancellation for cdma," *Communications, IEEE Transactions on*, vol. 46, pp. 258 –268, Feb 1998.

[12] C. Mensing, S. Sand, A. Dammann, and W. Utschick, "Interference-aware location estimation in cellular ofdm communications systems," in *Communications, 2009. ICC '09. IEEE International Conference on*, pp. 1 –6, June 2009.

[13] C. Mensing, S. Sand, A. Dammann, and W. Utschick, "Data-aided location estimation in cellular ofdm communications systems," in *Global Telecommunications Conference, 2009. GLOBECOM 2009. IEEE*, pp. 1 –7, Dec. 4 2009.

[14] European Telecommunications Standards Institute, *3GPP TS 36.211:"LTE;Evolved Universal Terrestrial Radio Access (E-UTRA);Physical channels and modulation"*, 10.1.0 release 10 ed., Apr 2011.

[15] D. Chu, "Polyphase codes with good periodic correlation properties (corresp.)," *Information Theory, IEEE Transactions on*, vol. 18, pp. 531 – 532, July 1972.

[16] European Telecommunications Standards Institute, *3GPP TS 36.355:"LTE;Evolved Universal Terrestrial Radio Access (E-UTRA);LTE Positioning Protocal(LPP)"*, 10.1.0 release 10 ed., Apr 2011.

[17] A. Dammann, C. Mensing, and S. Sand, "On the benefit of location and channel state information for synchronization in 3gpp-lte," in *Wireless Conference (EW), 2010 European*, pp. 711 –717, April 2010.

[18] A. Chandrakasan, W. Bowhill, and F. Fox, *Design of High-Performance Microprocessor Circuits*. Wiley-IEEE Press, 2000.

[19] C. F. Gerald and P. O. Wheatley, *Applied Numerical Analysis*. Addison-Wesley, 7 ed., 2004.

[20] A. Dammann, "Lecture notes: System aspects in signal processing." Technische Universität München, 2010.

[21] Wireless World Initiative - WWI, *WINNER II Deliverable D1.1.2: WINNER II channel models*.

[22] P. Hoeher, S. Kaiser, and P. Robertson, "Two-dimensional pilot-symbol-aided channel estimation by wiener filtering," in *Acoustics, Speech, and Signal Processing, 1997. ICASSP-97., 1997 IEEE International Conference on*, vol. 3, pp. 1845 –1848 vol.3, Apr 1997.

[23] K. Fazel and S. Kaiser, *Multi-Carrier and Spread Spectrum Systems*. New York, NY, USA: John Wiley & Sons, Inc., 2003.

[24] Y. Li, J. Cimini, L.J., and N. Sollenberger, "Robust channel estimation for ofdm systems with rapid dispersive fading channels," *Communications, IEEE Transactions on*, vol. 46, pp. 902 –915, July 1998.

[25] B. Fleury, M. Tschudin, R. Heddergott, D. Dahlhaus, and K. Ingeman Pedersen, "Channel parameter estimation in mobile radio environments using the sage algorithm," *Selected Areas in Communications, IEEE Journal on*, vol. 17, pp. 434 –450, Mar 1999.

[26] J. Fessler and A. Hero, "Space-alternating generalized expectation-maximization algorithm," *Signal Processing, IEEE Transactions on*, vol. 42, pp. 2664 –2677, Oct 1994.

[27] C. Günther, "Lecture script: Satellite navigation." Technische Universität München, 2010.

[28] C. Gentner and S. Sand, "NLOS detection and mitigation based on confidence metric and EKF," in *Proceedings of the ION 2011 International Technical Meeting (IMT)*, (San Diego, CA, USA), Jan. 2011.